



**HAL**  
open science

# Evaluation of Recycled Cardboard Paper as an Eco-Friendly Substrate for Rectenna and Ambient Radio Frequency Energy Harvesting Application

Pangsui Usifu Linge, Anvesh Pandey, Tony Gerges, Jean-Marc Duchamp, Philippe Benech, Jacque Verdier, Philippe Lombard, Fabien Mieyeville, Michel Cabrera, Pierre Tsafack, et al.

## ► To cite this version:

Pangsui Usifu Linge, Anvesh Pandey, Tony Gerges, Jean-Marc Duchamp, Philippe Benech, et al.. Evaluation of Recycled Cardboard Paper as an Eco-Friendly Substrate for Rectenna and Ambient Radio Frequency Energy Harvesting Application. *Electronics*, 2024, 13 (13), pp.2499. 10.3390/electronics13132499 . hal-04626085

**HAL Id: hal-04626085**

**<https://hal.science/hal-04626085v1>**

Submitted on 26 Jun 2024

**HAL** is a multi-disciplinary open access archive for the deposit and dissemination of scientific research documents, whether they are published or not. The documents may come from teaching and research institutions in France or abroad, or from public or private research centers.


L'archive ouverte pluridisciplinaire **HAL**, est destinée au dépôt et à la diffusion de documents scientifiques de niveau recherche, publiés ou non, émanant des établissements d'enseignement et de recherche français ou étrangers, des laboratoires publics ou privés.



Distributed under a Creative Commons Attribution - NoDerivatives 4.0 International License

## Article

# Evaluation of Recycled Cardboard Paper as an Eco-Friendly Substrate for Rectenna and Ambient Radio Frequency Energy Harvesting Application

Pangsui Usifu Linge<sup>1</sup>, Anvesh Pandey<sup>1</sup>, Tony Gerges<sup>1</sup>, Jean-Marc Duchamp<sup>2</sup>, Philippe Benech<sup>2</sup>, Jacques Verdier<sup>1</sup>, Philippe Lombard<sup>1</sup>, Fabien Mieyeville<sup>1</sup>, Michel Cabrera<sup>1</sup>, Pierre Tsafack<sup>3</sup> and Bruno Allard<sup>1,\*</sup> 

<sup>1</sup> Institut National des Sciences Appliquées de Lyon, Université Lyon1 Claude Bernard, Ecole Centrale de Lyon, CNRS, Ampere, UMR5005, F-6921 Villeurbanne, France; upangsuilingeh@gmail.com (P.U.L.); anveshpandey215@gmail.com (A.P.); gerges.tony@hotmail.com (T.G.); jacques.verdier@insa-lyon.fr (J.V.); philippe.lombard@univ-lyon1.fr (P.L.); fabien.mieyeville@univ-lyon1.fr (F.M.); michel.cabrera@insa-lyon.fr (M.C.)

<sup>2</sup> Univ. Grenoble-Alpes, CNRS, Grenoble INP, G2Elab, UMR5269, F-38000 Grenoble, France; jean-marc.duchamp@univ-grenoble-alpes.fr (J.-M.D.); philippe.benech@grenoble-inp.fr (P.B.)

<sup>3</sup> Depart. of Electrical and Electronic Engineering, Faculty of Engineering and Technology, Univ. Buea, Buea, Cameroon; tsafack.pierre@ubuea.cm

\* Correspondence: bruno.allard@insa-lyon.fr; Tel.: +33472438238

† Current address: INSA Lyon, Building Leonard de Vinci, 21 avenue Jean Capelle Ouest, F-69621 Villeurbanne, France

‡ These authors contributed equally to this work.

**Abstract:** Developers of electronics for the Internet of Things are considering nonstandard substrate materials like recyclable, low-cost, and eco-friendly cardboard paper. From this perspective, this article reviews the design and experimental results of a 2D-rectenna for scavenging radio-frequency energy at 2.45 GHz on various cardboard paper substrates for both the antenna and rectifier. Four types of recycled cardboard material, each with different thicknesses, air gaps, and surface roughness, are selected for characterization. A linearly polarized rectangular microstrip patch antenna with microstrip transmission feeding is adopted for ease of fabrication. At 2.45 GHz, the antenna has a simulated and measured global gain of 2.98 dB and 2.53 dB, respectively, on a 2.2 mm thick cardboard material. The rectifying element consists of a voltage-doubler configuration connected through a T-matching network to the antenna. At low RF input power (−10 dBm), the maximum available DC output power is experimentally evaluated at 1.73 μW, 7.5 μW, and 8.5 μW for HSMS-2860, HSMS-2850, and SMS7306-079L diodes, respectively. The respective rectifiers with diodes SMS7306-079L, HSMS-2850, and HSMS-2860 exhibit optimal load values of 2 kΩ, 2.6 kΩ, and 8 kΩ. The rectifier designed using the SMS7306-079L diode experimentally reaches a maximum power conversion efficiency (PCE) of 14.2% at -5 dBm input power when the optimal load value is 1.5 kΩ.

**Keywords:** cardboard paper; eco-friendly; low-cost; maximum power point; power conversion efficiency; radio frequency; rectenna; recyclable; two-transmission-line method



**Citation:** Linge, P.U.; Pandey, A.; Gerges, T.; Duchamp, J.; Benech, P.; Verdier, J.; Lombard, P.; Mieyeville, F.; Cabrera, M.; Tsafack, P.; Allard, B. Evaluation of Recycled Cardboard Paper as an Eco-Friendly Substrate for Rectenna and Ambient Radio Frequency Energy Harvesting Application. *Electronics* **2023**, *1*, 0. <https://doi.org/>

Academic Editor(s): Firstname  
Lastname

Received:

Revised:

Accepted:

Published:



**Copyright:** © 2023 by the authors. Licensee MDPI, Basel, Switzerland. This article is an open access article distributed under the terms and conditions of the Creative Commons Attribution (CC BY) license (<https://creativecommons.org/licenses/by/4.0/>).

## 1. Introduction

Continuous deposition of batteries in the environment causes environmental pollution [1]. This pollution does not decrease with the use of non-eco-friendly and nonrecyclable substrates in building radio frequency energy harvesting (RFEH) circuits. Ambient radio frequency energy harvesting becomes a significant candidate for supplying tiny electronic systems in areas where there is no practical access to sun, wind, or heat, or when objects are motionless. Even though the ambient RF environment is an ideal solution for energy harvesting due to a possibly continuous availability, it suffers from low incident power.

Broadband or multiband antennas are then used to increase the power conversion efficiency (PCE) of the rectenna [1]. As an example, the T-slot on the antenna further helps in achieving miniaturization but with a reduction in the antenna efficiency according to Babinet's principle. Metamaterials or metasurfaces can alternatively be used for achieving miniaturization [2]. Although this helps to increase the antenna gain, the substrate material may suffer from limitations concerning fabrication and recycling. The substrate negative relative permittivity affects computed antenna dimensions; hence, they change the impedance and resonance frequency of the antenna. Although metasurfaces can be used to build promising applications, metamaterials cannot be used easily in practice with cardboard material due to the high losses and severe dispersion associated with resonant responses [2].

RF energy harvesting circuits are often fabricated on standard but non-eco-friendly and nonrecyclable substrates. It is also hard to fold the majority of the latter substrates, so creating nonplanar 3D structures is difficult. Cardboard paper material is evaluated as a potential substrate for accessing nonflat substrates. Cardboard is more or less an ecofriendly, recyclable, biosourced material which can be folded into rather complex shapes and forms. Figure 1 reviews the recent state of the art on RF energy harvesting systems. A rectenna on polyethylene terephthalate (PET) offers significant performance results [3] but PET is not recyclable so far. Paper substrate rectennas have been reported as well [3–5,10]. The rectifier in [5] is designed for an input power of -20 dBm, using HSMS-282B diodes as rectifying elements in a five-stage Villard topology, with a PCE of 58%. The fabrication on paper often uses conductive ink and the fabricated object may not be easily recycled.

Polylactic acid (PLA) is an ecofriendly material reported for rectenna design [6]. PLA is compatible with additive manufacturing like 3D printing or fuse deposition modeling (FDM). The major disadvantage of FDM is the surface roughness of the finished structures. FDM is also more expensive compared to structuring elementary circuits on cardboard paper.

The use of cardboard materials has several limitations, including high surface roughness, porosity, high losses, and limited lifespan of circuits constructed on the soft material. From the perspective of rapid prototyping, RF circuits are created using copper tape of a thickness of 35  $\mu\text{m}$  (3M company, Saint Paul, Minnesota, USA). Commercial copper tape comes with glue on one surface, which creates an immediate and smooth attachment to the substrate's outside surface. The copper tape may be quite easily removed from the substrate as a first step in the dismantlement of the circuit.

There is an interest in investigating the "low-tech" fabrication of RFEH to be added to cardboard objects for supplying tiny sensors or functions. This paper's objective is to document the essential RF parameters for design, the order of magnitude of antenna performances, and rectifier efficiency. No original contribution is presented at the design level but the design approaches are experimentally verified with regards to cardboard material. Conclusions may be drawn on the power supply capability of a tiny intermittent electronic system. This paper's content is organized as follows. In Section 2, the two-transmission-line (TTL) method is used for extracting the major RF properties of the cardboard paper substrates. The surface roughness of various types of cardboard papers is the focus. The extracted results (loss tangent and relative permittivity) are discussed. Section 3 details the fabrication and measurement results for patch antennas. The impact of the cardboard substrate is discussed. Section 4 discusses the characterization of a one-stage voltage-doubler rectifier on selected cardboard paper substrates. Section 5 covers conclusions and perspectives.

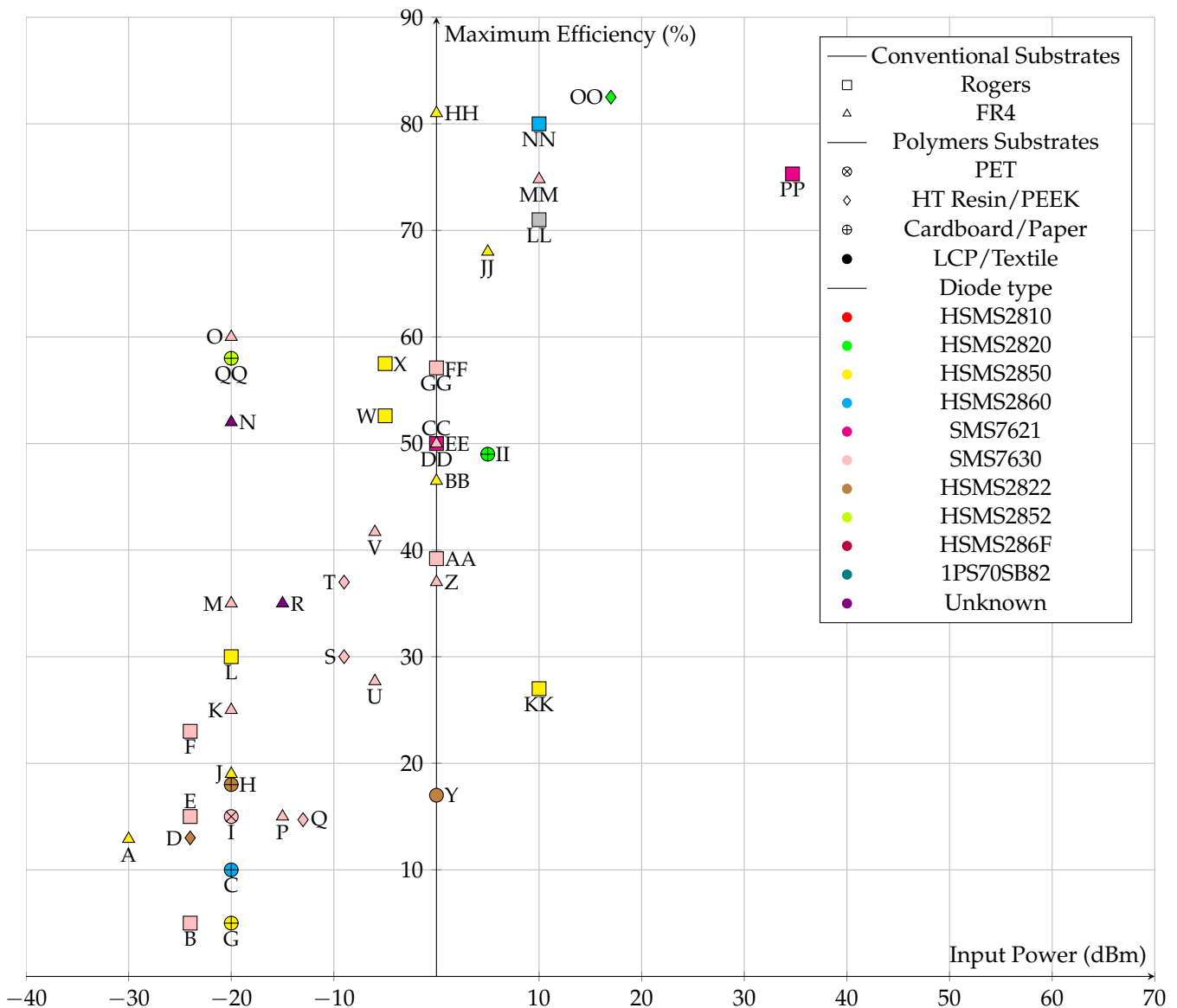


**Figure 1.** Recent state of the art: maximum efficiency vs. input power depending on substrate type and diode reference. A—[7], B—[8], C—[10], D—[9], E—[8], F—[8], G—[10], H—[4], I—[3], J—[11], K—[12], L—[13], M—[12], N—[14], O—[12], P—[15], Q—[16], R—[14], S—[17], T—[17], W—[18], X—[18], Y—[19], Z—[20], AA—[21], BB—[22], CC—[22], DD—[23], EE—[24], FF—[25], GG—[21], HH—[26], II—[27], JJ—[11], KK—[28], LL—[29], MM—[20], NN—[30], OO—[12], PP—[31], QQ—[5].

## 2. Substrate Characterization

One of the most essential properties required is a nonconductive substrate. The RF properties of the substrate are fundamental in designing RF systems. In this section, we utilize the two-transmission-line (TTL) method to extract the loss tangent and relative permittivity of cardboard substrates. The TTL method is a simple method deployed over a wide band of frequency. The details of the TTL are described in the literature [6,32].

### 2.1. TTL Method on Cardboard Substrate

There are many types of cardboard materials with different air gaps, thicknesses, and surface roughness. Four cardboard materials with varying thickness, air gap densities, and surface roughness are selected for characterization (Figure 2): raw materials supply sample #1 with a thickness of 2.2 mm, sample #2 with a thickness of 2.15 mm, sample #3 with a thickness of 3.6 mm, and sample #4 with a thickness 1.7 mm. The samples were

observed through a Stemi 305 microscope to quantify the level of air gap density. The images are shown in Figure 3. It was found that samples #1 and #4 presented higher mass density compared to other materials and, thus, will be selected for the final tests. Moreover, Figure 2a shows that sample #1 presents a thin color coating on one side, which gives a surface of less roughness than the other, and both surfaces will be evaluated.



**Figure 2.** Different cardboard raw materials: (a) sample #1 (2.2 mm thickness), (b) sample #2 (2.15 mm), (c) sample #3 (3.6 mm), (d) sample #4 (1.7 mm).

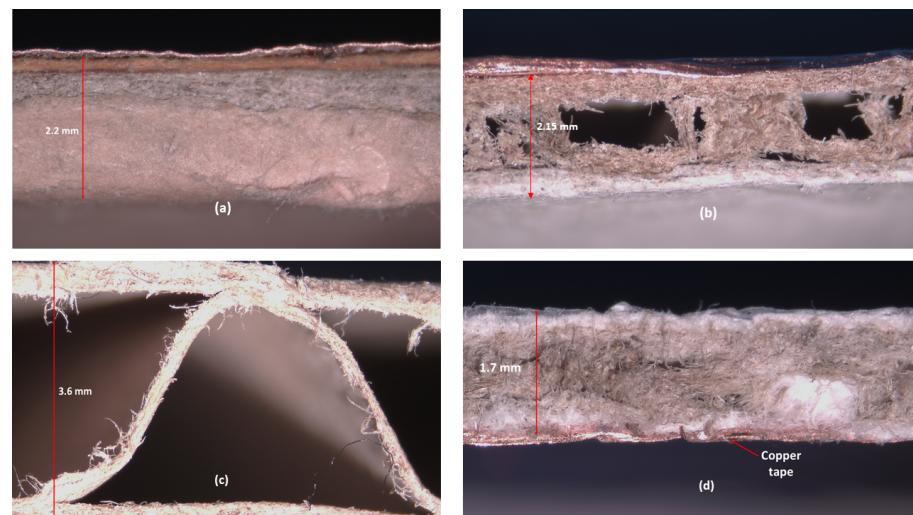


**Figure 3.** Different cardboard samples were observed under the microscope: (a) sample #1, (b) sample #2, (c) sample #3, (d) sample #4.

## 2.2. Physical Properties

The mass densities of the cardboard samples #1, #2, #3, and #4 are  $696 \text{ kg/m}^3$ ,  $182 \text{ kg/m}^3$ ,  $139 \text{ kg/m}^3$ , and  $434 \text{ kg/m}^3$ , respectively. The cardboard samples #2 and #3 have more air gaps than samples #1 and #4. The cardboard sample #1 is affected by the fewest air gaps. The roughness of the used conductor (copper tape) on each cardboard sample was measured using a nano-point-scanner (NPS) with a zooming scale of

600  $\mu\text{m}$ . Figure 4 displays the surface roughness observed for each sample under the Hirox microscope. The average roughness was calculated after conducting three roughness measurements on each sample. Cardboard materials are soft, so three measurements in different areas of the sample were considered to provide significant information. The results are listed in Table 1, and Figure 5 shows the minimum, maximum, and average roughness values for each cardboard sample.

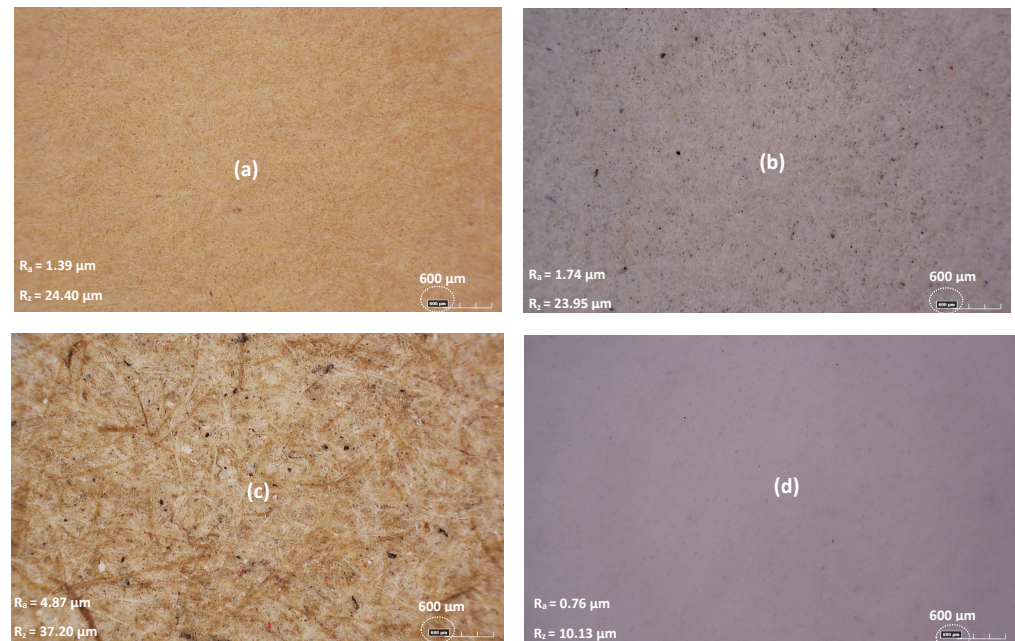


**Figure 4.** The surface roughness of different cardboard samples observed under Hirox microscope: (a) sample #1, (b) sample #2, (c) sample #3, (d) sample #4.

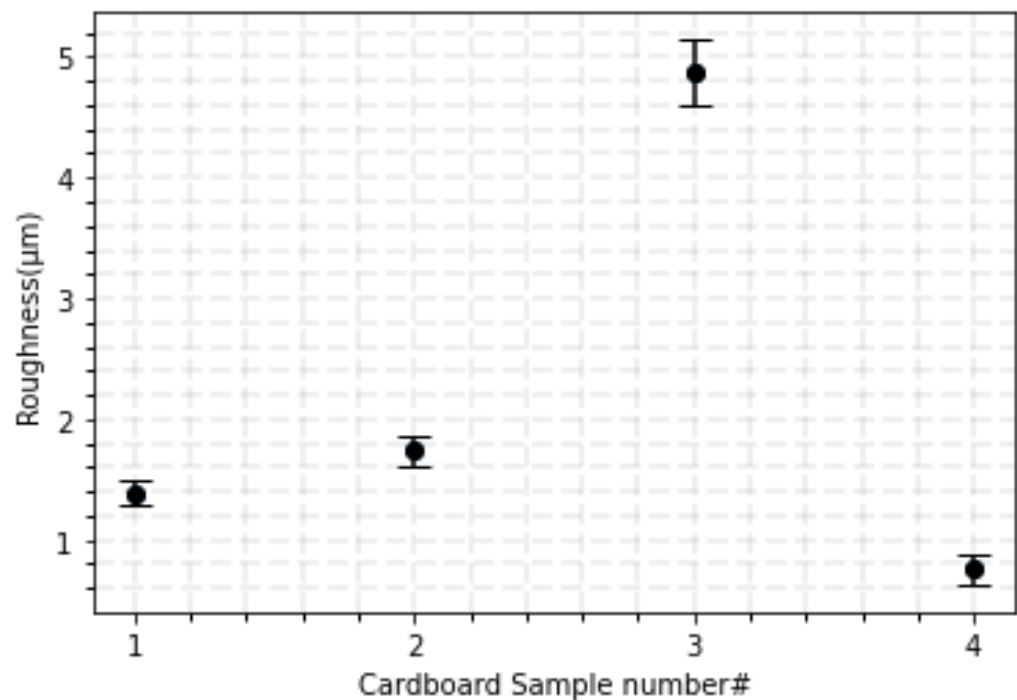


**Figure 5.** Plot depicting the range of roughness values for each cardboard sample.

**Table 1.** Roughness measurement of the different cardboard samples.

Sample Name	Measurement 1 ( $\mu\text{m}$ )	Measurement 2 ( $\mu\text{m}$ )	Measurement 3 ( $\mu\text{m}$ )	Average ( $\mu\text{m}$ )
Sample #1	1.34	1.45	1.38	1.39
Sample #1 ground	3.14	3.53	3.85	3.50
Copper tape on Sample #1	0.82	0.63	0.74	0.73
Sample #2	1.79	1.76	1.67	1.74
Sample #2 ground	4.56	4.68	4.9	4.71
Copper tape on Sample #2	0.59	0.61	0.6	0.6
Sample #3	5	4.73	4.89	4.87
Sample #3 ground	4.8	5.2	4.9	4.97
Sample #4	0.69	0.82	0.78	0.76
Sample #4 ground	2.7	3.2	3.27	3.06

Table 1 shows that the cardboard samples #2 and #3 have the highest surface roughness while the sample #4 has the lowest value. This is due to a smooth plastic coating of thickness 0.1 mm on sample #4. The roughness of cardboard sample #1 is slightly higher than that of sample #4. However, the cardboard sample #1 has the most limited quantity of air gaps. There is a trade-off between the roughness and the air gaps. The air gaps make the substrate more fragile and decrease its relative permittivity. Moisture may also be a contaminant that affects permittivity. As a result, the energy related to the electric field in the substrate material is reduced. In addition, the air gaps also introduce geometric imperfections in the substrate, leading to variations in the loss tangent and dielectric constant of the substrates. Cardboard sample #1 is most suitable for this work.

Table 1 also shows that the roughness values for the two surfaces (front and ground plane) on the same sample differ. This difference is due to the presence of the coating on only one side of the cardboard substrates. In conclusion, the average roughness values when considering both surfaces of the cardboard samples #1, #2, #3, and #4 are 2.415  $\mu\text{m}$ , 3.15  $\mu\text{m}$ , 4.735  $\mu\text{m}$ , and 1.91  $\mu\text{m}$ , respectively.

### 2.3. Relative Permittivity and Loss Tangent of Cardboard Material Substrates

The main RF properties of interest here are the loss tangent and the relative permittivity. Cardboard samples are manufactured for the two-transmission-line (TTL) method as shown in Figure 6. The lines are fabricated using a commercial copper tape of thickness 35  $\mu\text{m}$ .

It was verified that the input impedance of the lines was always as close to 50  $\Omega$  as possible. The effect of the SMA connectors was investigated by interchanging the ports during measurements. In all cases,  $S_{12}$  was always equal to  $S_{21}$ . A small variation was observed in the case of  $S_{11}$  and  $S_{22}$ . This might be due to geometric imperfections in the sample manufacturing, as this effect is not significant with the Rogers RO4003C substrate. However, it is worth noting that the effects of SMA connectors and junctions are corrected by the TTL method providing that they are strictly similar [33,34]. Manual soldering of SMA connectors introduces a slight variability.

The experimental values of the loss tangent and dielectric constant are comparable to values obtained from the literature (Table 2). The RF properties of the cardboard materials are directly affected by the number of air gaps in them. As the quantity of air gaps increases, the relative permittivity decreases, thereby approaching the dielectric constant of air. This explains why the cardboard samples #2 and #3 have lower values of relative permittivity and higher values of loss tangent. Cardboard sample #1 shows the highest value of relative permittivity due to its limited number of air gaps. The loss tangent is also lower due to a coating on both surfaces. However, these coatings are a bit rougher than the plastic coating on the cardboard sample #4. The value of the loss tangent of cardboard sample #4 is slightly

lower than that of cardboard sample #1. This is due to the presence of a smoother plastic coating on the upper surface of the cardboard sample #4.

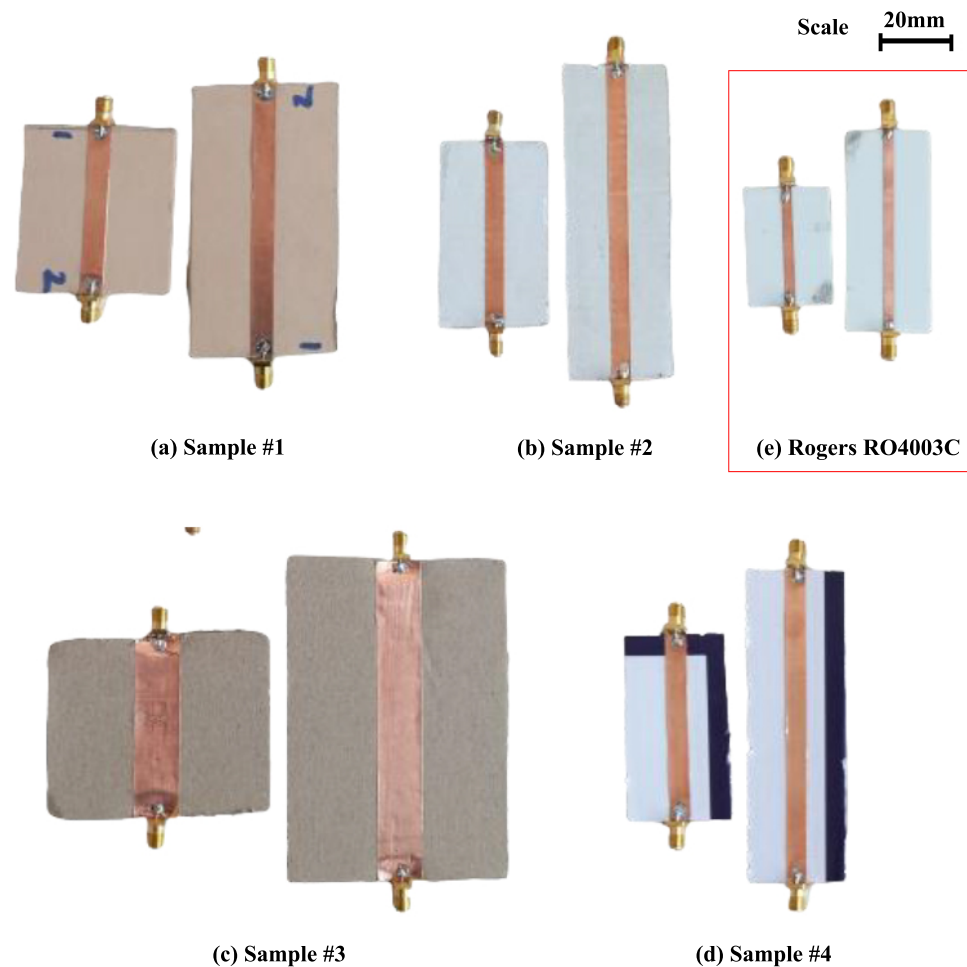


**Figure 6.** Devices for the two-transmission-line method on the substrate: (a) sample #1, (b) sample #2, (c) sample #3, (d) sample #4, and (e) Rogers RO4003C as a reference sample.

**Table 2.** Dielectric permittivity and loss tangents of cardboard paper substrates as compared with the literature.

Frequency (GHz)	$L_1/L_2$ (mm)	Thickness (mm)	$\tan\delta$	$\epsilon_r$	Method	Ref
0.5–3	30/100	2.9	0.04–0.08	1.4–2.6	Coplanar Wave-guides	[5]
0.5–3	50/100	0.56	0.015–0.028	1.78–1.82	TTL	[35]
0.5–3	55.5/91	2.2	0.054–0.057	1.889–1.968	TTL	sample #1
0.5–3	60/100	2.15	0.01–0.07	1.189–1.264	TTL	sample #2
0.5–3	67/108	3.6	0.025–0.08	1.17–1.24	TTL	sample #3
0.5–3	65/108	1.7	0.045–0.065	1.401–1.415	TTL	sample #4

### 3. Antenna

The material RF properties enable the design of the antenna. The goal of this section is not to propose a particular antenna geometry but to investigate the performance of the



simple microstrip patch antenna [36,37] with respect to the substrate and with regards to rapid prototyping. In addition, patch antennas have simple profiles and are suitable for both planar and nonplanar surfaces [38–46]. The length and width of a rectangular patch are approximated using Equations (1) and (2) [37,47].

$$L = \frac{\lambda_0}{2} - 2\Delta L \quad (1)$$

$$W = \frac{1}{2f_r\sqrt{\mu_0\epsilon_0}}\sqrt{\frac{2}{\epsilon_r + 1}} \quad (2)$$

where

$$\Delta L = 0.412 h(\epsilon_{reff} + 0.3) \left(\frac{W}{h} + 0.264\right) / (\epsilon_{reff} - 0.258) \left(\frac{W}{h} + 0.8\right) \quad (3)$$

and

$$\epsilon_{reff} = \frac{\epsilon_r + 1}{2} + \frac{\epsilon_r - 1}{2} \left[1 + 12\frac{h}{W}\right]^{-\frac{1}{2}} \quad (4)$$

$\lambda_0$ ,  $\epsilon_r$ , and  $f_0$  are the wavelength, the dielectric constant of the substrate, and the operating frequency, respectively.  $\Delta L$  and  $\epsilon_{reff}$  denote the length extension and the effective dielectric constant of the antenna due to the fringing effect, and  $h$  is the thickness of the substrate.

### 3.1. Effect of Losses and Dielectric Constant on the Antenna Parameters

Due to the asymmetrical dimension of the substrate, it is important to study the influence of the losses and the relative permittivity on the radiation parameters of the antenna. Some areas of the substrate have more air gaps than others, causing fluctuations in the values of the loss tangent and the relative permittivity along the substrate. In addition, the cardboard material can absorb humidity from the environment, thereby altering its physical and RF parameter values. Figures 7 and 8 show simulation evaluations of how variations in the loss tangent and dielectric constant affect the antenna's electrical impedance. Tables 3 and 4 summarize the alteration of the antenna global gain in response to the variation in dielectric constant and losses of the substrate, respectively.

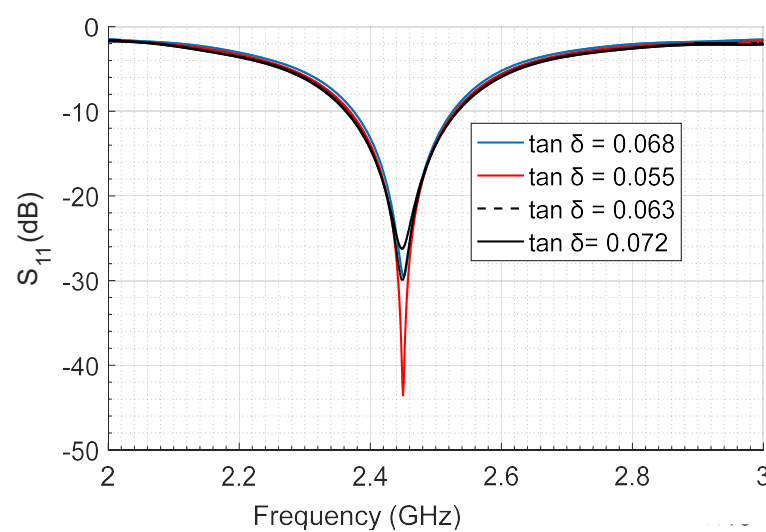
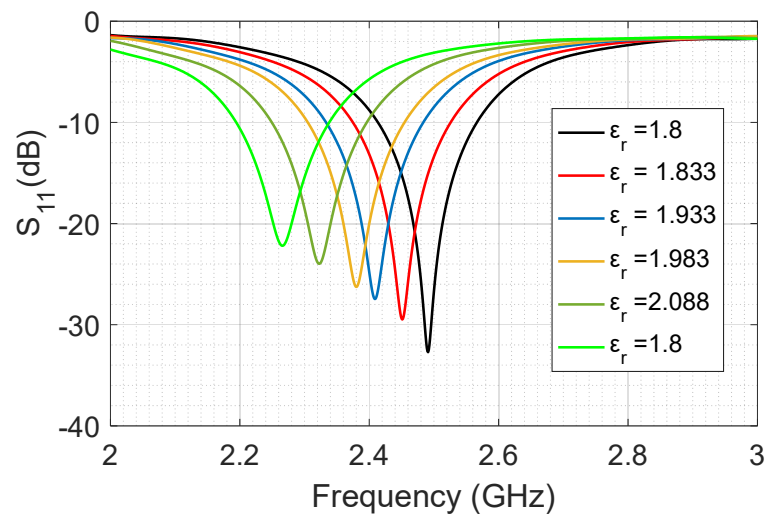


Figure 7. CST simulation results:  $S_{11}$  variation according to the losses of the cardboard substrate.



**Figure 8.** CST simulation results:  $S_{11}$  variation according to the relative permittivity of the cardboard substrate.

**Table 3.** Simulated effect of loss tangent on antenna global gain (cardboard sample #1, dielectric constant 1.8333).

Loss tangent ( $\tan\delta$ )	Recessed Distance (mm)	$S_{11}$ (dB)	Gain (dB)	Bandwidth (MHz)	Efficiency (%)
0.055	2.7	-43.5	2.46	146.5	33.9
0.063	1.5	-30	2.03	154	31
0.068	0.8	-29.85	1.78	158.2	29.35
0.072	—	-26.34	1.58	160.4	28.14

**Table 4.** Simulated effect of dielectric constant on antenna global gain (cardboard sample #1, loss tangent 0.055).

Dielectric Constant ( $\epsilon_r$ )	Length of Patch (mm)	$S_{11}$ (dB)	Gain (dB)	Bandwidth (MHz)	Efficiency (%)
1.8	43.40	-33.45	2.46	147.9	34
1.833	—	-28.85	2.54	146.6	33.7
1.933	—	-27.25	2.29	142.8	33.4
1.963	41.70	-26.10	1.88	142	33.1
2.088	39.5	-24.13	0.319	138.1	32.8

In Table 3, as the loss tangent decreases,  $S_{11}$  becomes better. In Figure 8, the values of  $S_{11}$  shift to the left as the relative permittivity decreases. This is because the electrical length of the patch increases as the dielectric constant decreases. This latter increase in electrical length causes the minimum value of the  $S_{11}$  parameter to shift to a lower frequency.

The cardboard material is not very homogeneous and the RF properties may vary across the area. The impact of varying dielectric constant values and loss tangent values impact the geometry of the antenna. Considering worst-case and best-case values, the latter impact is shown in Figure 9 and Figure 10, respectively. As the dielectric constant increases, the desired resonant frequency changes. To resonate the antenna at the desired frequency, the length of the patch should be reduced (Figure 4). The variation in the dielectric constant affects only the length of the patch antenna, while all other dimensions remain constant. A comparable pattern is noticed with variations in the losses of the substrate. As the loss

tangent increases, the desired resonant frequency remains unchanged, but the matching becomes destabilized with an upward shift in the return loss. To improve the return loss value, the recessed distance ( $W_C$ ) should be reduced (Figure 10). In conclusion, great care must be taken during the manufacturing of the antenna and rectifier to keep the substrate as pristine as possible.

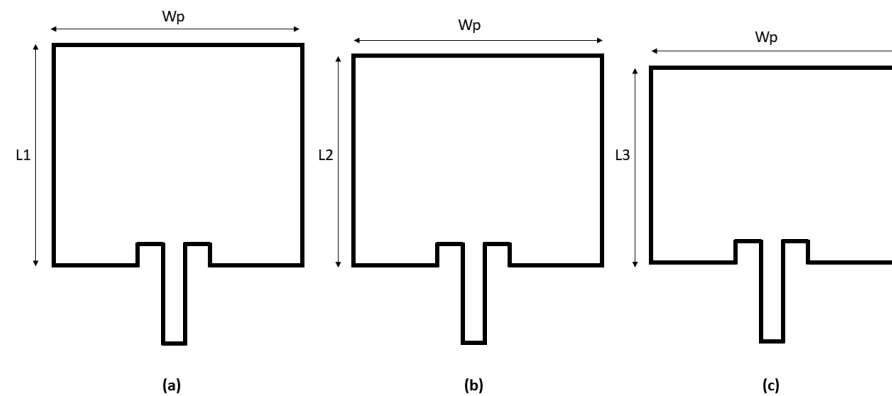


**Figure 9.** Impact on antenna geometry of varying dielectric constant value ((a)  $L_1 = 43.40$  mm, (b)  $L_2 = 41.70$  mm, and (c)  $L_3 = 39.5$  mm are the lengths of the patch with a dielectric constant of 1.833, 1.983, and 2.2, respectively).

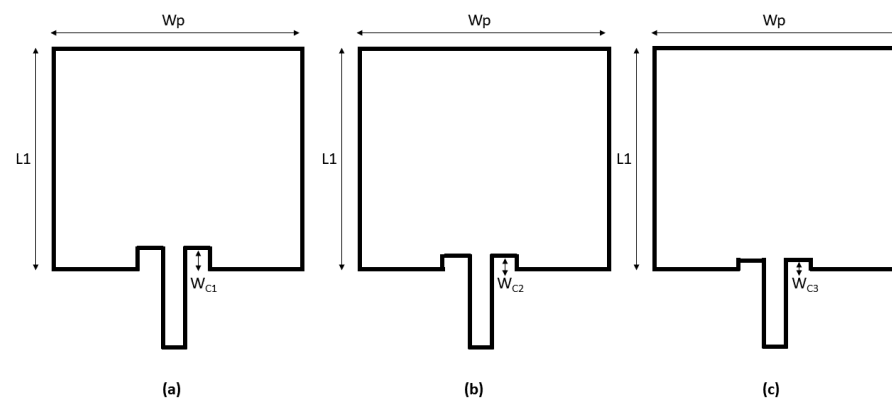


**Figure 10.** Impact on antenna geometry of loss tangent value ((a)  $W_{C1} = 2.7$  mm, (b)  $W_{C2} = 1.5$  mm, and (c)  $W_{C3} = 0.8$  mm are the lengths of the inset with loss tangent of 0.055, 0.063, and 0.068, respectively).

From Table 4, as the dielectric constant increases, radiation parameters decrease. This observation is in agreement with the results obtained in [48,49]. As the losses increase, the gain,  $S_{11}$ , and efficiency of the patch decrease (Table 3).

### 3.2. Effect of Substrate Thickness on Antenna Parameters

Since there are various categories of cardboard with different thicknesses, it is important to study how the thickness affects the parameters of the antenna. The simulated variation of the radiation pattern of the antenna with the thickness of the substrate is summarized in Table 5. The antenna efficiency can be increased by as much as 90% and its bandwidth by 35% in the absence of surface waves [50]. However, as the antenna height increases, surface waves appear, and these are often undesirable as they absorb part of the power that was injected for direct radiation. Surface waves propagate through the substrate and disperse at bends and surface discontinuities such as the ground plane and dielectric truncation; they impair the antenna pattern and polarization properties. Surface wave elimination allows broad bandwidth and efficiency. Applying cavities to the substrate is one way to achieve this [50].

**Table 5.** Simulated effect of cardboard substrate thickness on antenna radiation parameters (cardboard sample #1, loss tangent 0.055).

Thickness (mm)	$\epsilon_r$	Lp (mm)	Wp (mm)	S <sub>11</sub> (dB)	Gain (dB)	Bandwidth (MHz)	Efficiency (%)
2.15	1.87	43.2	54	−34.4	1.84	140.4	32.12
1.7	1.86	43.2	54	−48.7	2.47	146	33.88
2.2	1.85	43.2	54	−27.3	2.9	157.9	39.55
3.6	1.81	43.2	54	−16.8	3.6	166.2	52.14

When considering losses in the antenna, the global gain, the efficiency, and the bandwidth increase as the thickness of the substrate increases. This aligns with the results presented in [50]. However, simulations performed with larger thicknesses revealed a decrease in gain and efficiency. This decline is associated with the introduction of surface waves that degrade the antenna radiation parameters [50].

### 3.3. Single Band Antenna

A single-band antenna at 2.45 GHz is simulated using CST Microwave software with the identified values of  $\tan\delta$  and  $\epsilon_r$ . A microstrip feed line is considered for the ease of matching to 50  $\Omega$  by tuning the insertion position. To match the antenna to a 50  $\Omega$  input impedance, a recessed distance H from one edge is calculated using Equation (5) and later optimized with CST Microwave Studio (Figure 11a). This creates two physical notches that introduce two junction capacitors [50]. These capacitors can slightly influence the resonance frequency.

$$H = \frac{0.822 * L}{2} \quad (5)$$

where  $L$  is the length of the patch antenna.

The geometry of the antenna and the fabricated patches on cardboard samples #1 and #4 are shown in Figure 11, respectively. The patch fabricated on the smoother face of cardboard material #1 is denoted #1a. To further verify the impact of losses due to the roughness of the cardboard, a similar patch was fabricated on the rougher side of cardboard sample #1, denoted #1b.

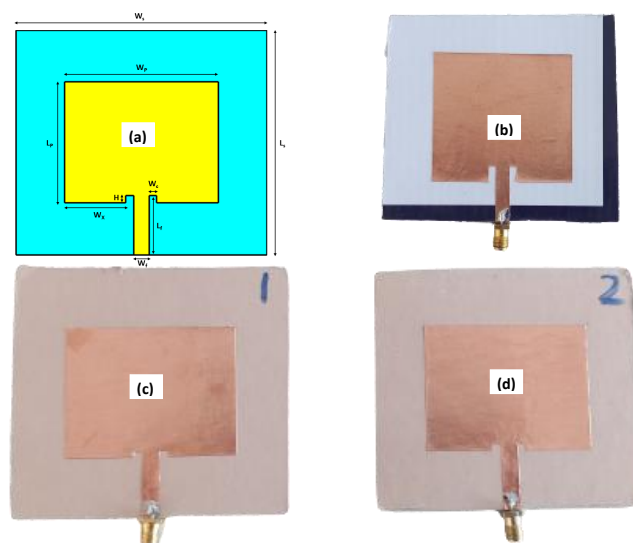


**Figure 11.** Patch antenna manufactured on cardboard substrate using copper tape as the conductive material. (a) Geometry (with parameters in Table 6), (b) fabricated patch on cardboard sample #4, (c) fabricated patch on cardboard sample #1a, (d) fabricated patch on cardboard sample #1b.

**Table 6.** Antenna geometry (in mm) in Figure 11.

Sample Name	Wp	Lp	Wf	Lf	Wx	Wc	Ws	Ls	H
Sample #1	54	41.5	5.4	21	21.6	2.7	88	80	1.9
Sample #4	54	41.5	5.4	21	21.6	2.7	88	80	5.9

The simulated and measured  $S_{11}$  results are shown in Figure 12 and Figure 13, respectively, for cardboard sample #4 and cardboard sample #1a (smooth surface) and #1b (rougher surface), respectively. Figure 13 shows a slight variation between the two fabricated patches of the same geometry. This result is unexpected and one assumption is that applying the copper tape without a dedicated tool may not be an accurate and repetitive fabrication approach. An inaccuracy could arise that would mask the difference in behavior resulting from the substrate face roughness. Equations (6) and (7) show the relationship between the length and width of the substrate as a function of the resonance frequency.

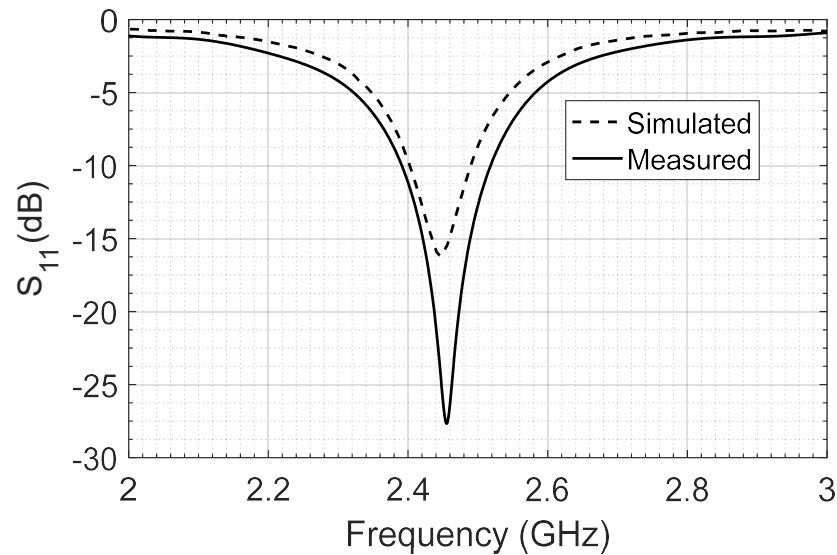
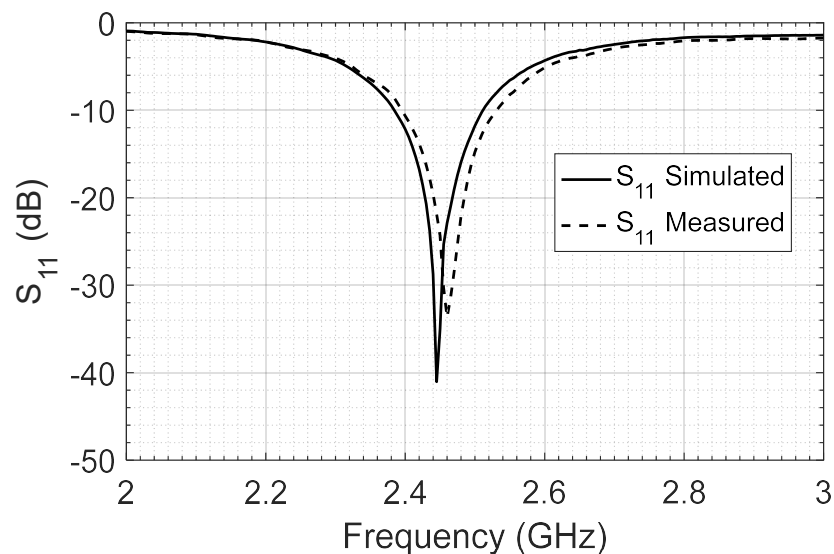
**Figure 12.** Simulated and measured  $S_{11}$  of the antenna on cardboard sample #4 (Figure 11b).**Figure 13.** Simulated and measured  $S_{11}$  of antenna on cardboard sample #1a (Figure 11c).

Figure 13 also shows that the antenna on cardboard sample #1b (rougher surface) presents more losses than the same patch antenna fabricated on a smoother surface. In any case, both samples offer good agreement between simulated and measured results.

$$L_s = 6 h + \frac{C_0}{2f_r \sqrt{\epsilon_{\text{reff}}}} - 2\Delta L \quad (6)$$

$$W_s = 6 h + \frac{C_0}{2f_r} \sqrt{\frac{2}{\epsilon_r + 1}} \quad (7)$$

Table 7 lists the main parameters of simulated and fabricated antennas on sample #1 and sample #4. The simulation does not account for additional losses related to the roughness of the substrate receiving the patch geometry. All losses are considered, and the realized gain is mentioned in decibels (dB). Sample #4 yields better results for the patch antenna. As the patch geometry increases, the realized gain decreases. The antenna exhibits a better gain value at 2.4 GHz than 900 MHz. The agreement between simulation and experiment is the best at 2.45 GHz which indicates a larger spread of RF properties with frequency.

**Table 7.** Main properties of patch antenna fabricated on cardboard substrates.

Sample Number	Size (mm <sup>3</sup> )	Gain (dB)	Bandwidth (MHz)	Resonance Frequency (GHz)	S <sub>11</sub> (dB)
#4 simulation	80 × 88 × 1.7	3.12	136.8	2.4523	−37.098
#4 measurement	80 × 88 × 1.7	3.01	109	2.446	−16.204
#1 simulation	80 × 88 × 2.2	2.98	169.9	2.4513	−39.76
#1a measurement	80 × 88 × 2.2	2.53	160.4	2.46	−33.653
#1b measurement	80 × 88 × 2.2	2.51	168.7	2.45	−25.98
#1 simulation	190 × 186 × 2.2	0.21	20	0.900	−11.387
#1a measurement	190 × 186 × 2.2	0.45	25	0.900	−14.15
#1a simulation	190 × 186 × 2.2	0.369	107.2	1.816	−12.847
#1a measurement	190 × 186 × 2.2	0.54	120	1.862	−21.15

Sample #1a fabricated on smooth (front) face (Figure 11c); sample #1b fabricated on rough (back) face (Figure 11d).

### 3.4. Dual-Band Antenna

An antenna resonating at 900 and 1800 MHz, respectively, is simulated using cardboard sample #1a (smoother face) RF properties. Since this antenna can capture the RF signals at two different frequencies, it can lead to a higher PCE of the rectenna circuit. The geometry and fabricated patches are shown in Figure 14. The dual-band capability is achieved by shifting the feed line to the left, resulting in unequal widths  $W_{X1}$  and  $W_{X2}$ . The radiation parameters of the antenna at both frequencies are shown in Table 7.

The simulated and measured  $S_{11}$  are shown in Figure 15. There is an agreement between the simulated and the measured values at 900 MHz, with the simulation slightly outperforming the measurement. However, at 1800 MHz, there is a small difference between simulation and measurement. Nevertheless, the agreement between the simulated and measured results at the frequency of interest indicates that the extracted loss tangent and the relative permittivity values are acceptable and may be used for designing RF circuits on cardboard materials.

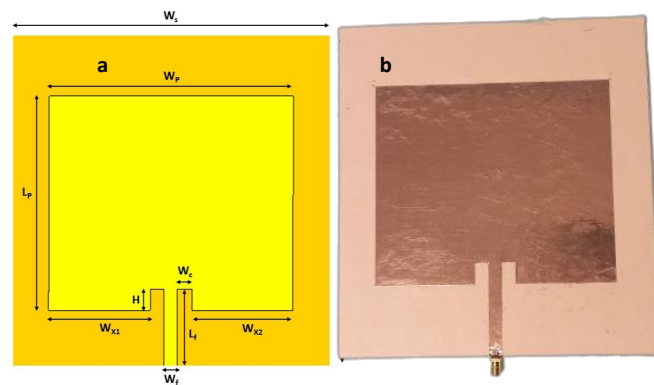


**Figure 14.** Dual-band patch antenna fabricated on cardboard sample #1a (smoother face): (a) geometry (with parameters in Table 8), (b) fabricated patch.

**Table 8.** Geometry (in mm) of antenna in Figure 14 on cardboard sample #1a substrate.

$W_p$	$L_p$	$W_f$	$L_f$	$W_{x1}$	$W_{x2}$	$W_c$	$W_s$	$L_s$	$H$
152	108.1	7.6	47	64.2	63.7	8	186	190	2.2

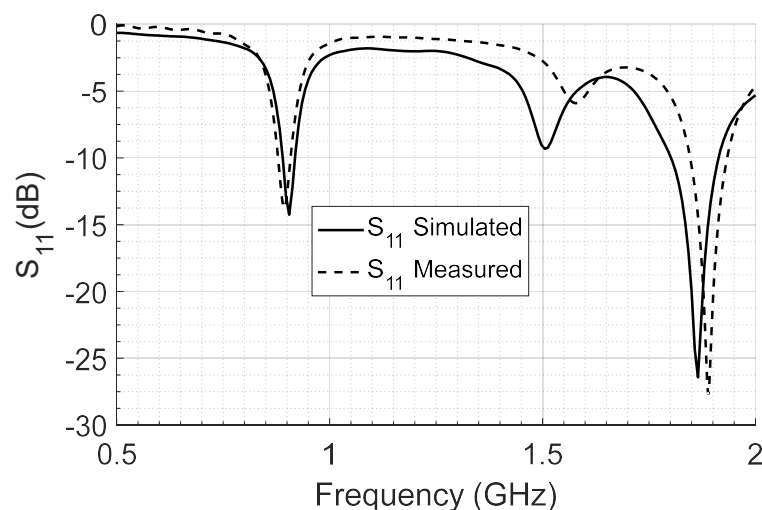


**Figure 15.** Simulated and measured return loss of dual band patch antenna on cardboard sample #1a (smooth face).

### 3.5. Broadband Antenna

Broadband antennas offer the advantage of operating over a wide range of frequencies, enabling them to capture signals at various frequencies effectively. With the increased intensity of the captured signal, the PCE of the rectenna circuit should increase. However, the main challenge of broadband antenna is matching them to the rectifier. In this work, generating the broadband antenna is performed by creating slots on the patch plane. The truncated ground plane, a well-known technique, was investigated to assess whether the cardboard paper substrate interferes with this technique. The resulting structure is a monopole antenna. A negative effect of slots on the ground plane in gain reduction occurs due to the introduction of back radiation and disturbance in the current distribution on the ground plane [2]. The antenna was simulated in CST design software and fabricated on cardboard sample #1 (smooth face). The geometry and fabricated monopole are shown in Figure 16. Two identical antennas were fabricated to facilitate the gain measurement later

using the “two-identical antenna method” based on Friis free space equation. The length and width of the monopole are calculated using Equation (8).

$$L = W = \lambda/4 \tag{8}$$

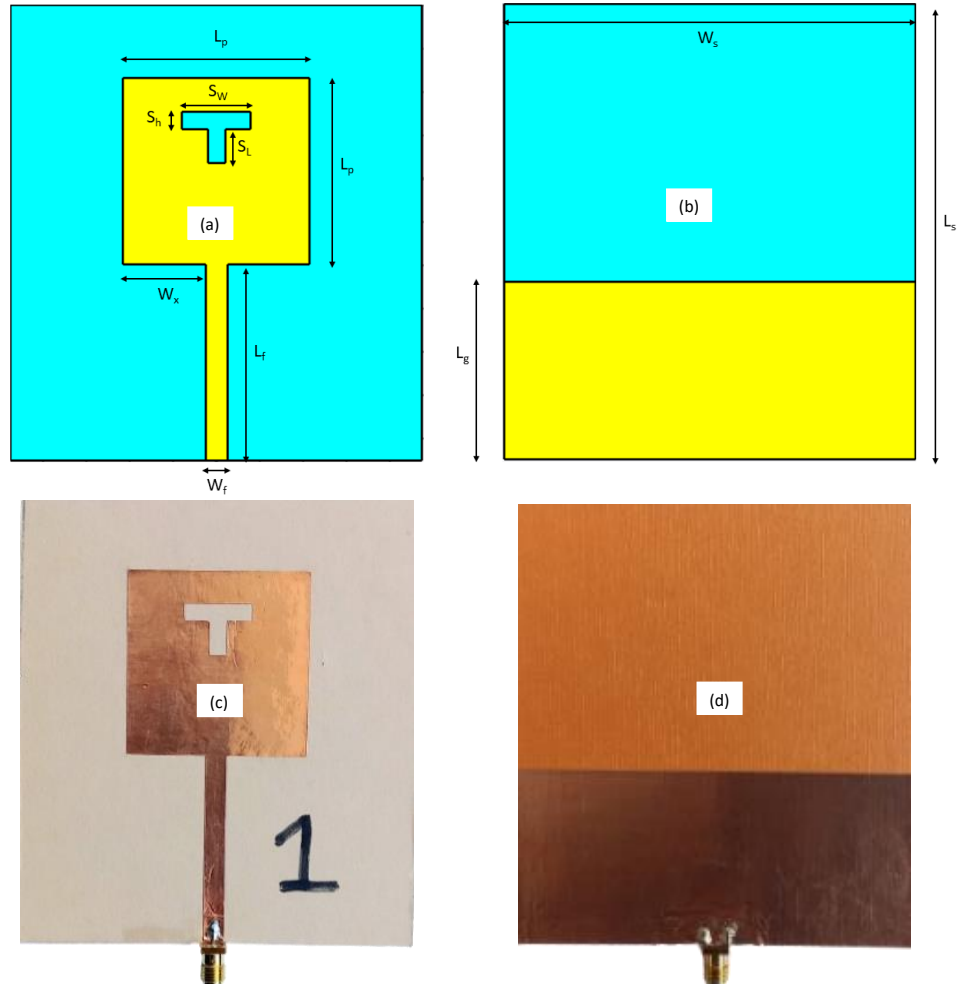


**Figure 16.** Monopole antenna fabricated on cardboard sample #1 (smooth face). (a) Geometry of front view (with parameters in Table 9), (b) back view (ground plane), (c) printed monopole (front view), (d) printed monopole (ground plane).

**Table 9.** Geometry (in mm) of the antenna in Figure 16 on cardboard sample #1a substrate.

$L_p$	$L_s$	$L_g$	$W_s$	$W_x$	$L_f$	$S_h$	$S_w$	$S_l$	$W_f$
43	105	41	95	19	45.1	4	16	6	5

The resonance frequency is fixed at a chosen value and Equation (8) is applied, corresponding to the first frequency peak in Figure 17. The bandwidth is increased on both sides of the fixed value by using a partial ground plane around the length of the monopole. Further bandwidth enlargement is achieved by adding a T-slot on the patch.

The simulated and measured return loss for the antenna are shown in Figure 17, and radiation parameters of the antenna are summarized in Table 10.



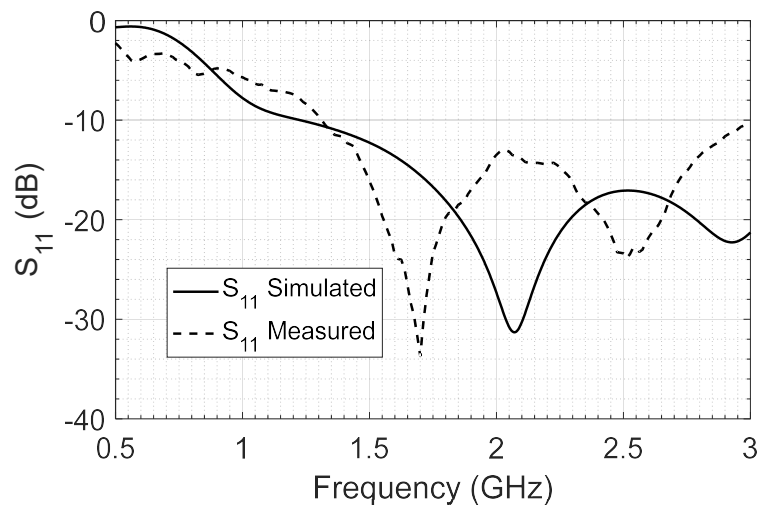


**Figure 17.** Simulated and measured return loss of broadband monopole antenna on cardboard sample #1a (smooth face).

**Table 10.** Main properties of monopole antenna fabricated on cardboard paper substrate sample #1a (smooth face).

Sample Number	Global Gain (dB) at 2.45 GHz	Bandwidth (MHz)	S <sub>11</sub> (dB) at 2.45 GHz	Size (mm <sup>3</sup> )
#1 simulation	2.51	2010.2	−16.519	105 × 95 × 2.2
#1 measurement	2.2	2132	−22.23	105 × 95 × 2.2

As observed in Figure 17, there are some discrepancies between the simulated and the measured results. Specifically, there is a shift to the left for the measured result. The difference can be attributed to the effective permittivity of the substrate. The simulation can be adjusted by changing the permittivity to shift the simulated S<sub>11</sub> frequency. At 2.45 GHz, the return loss values are −16.5 dB and −22.2 dB for simulation and measurement, respectively.

#### 4. Rectifier

The rectifier is responsible for converting the RF signals into DC current and voltage for supplying the consumption load. In the case where the DC power at the rectifier output is not suitable for the load, an optional power management unit (PMU) is added between the rectifier and the load (Figure 18). The PMU is a more or less complex DC–DC converter.

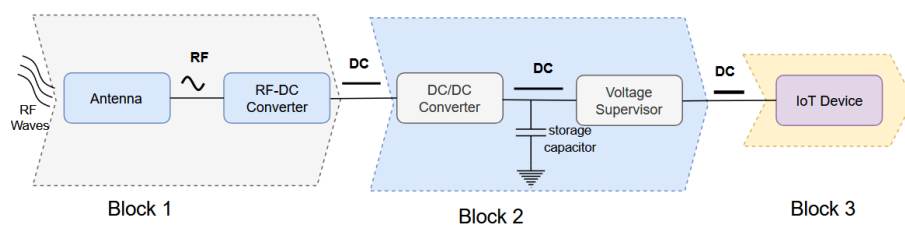


**Figure 18.** Block diagram of a rectenna with an optional PMU.

The PCE of the rectifier depends on the zero-bias junction capacitor,  $C_{j0}$ , the breakdown voltage,  $V_{br}$ , and the series resistor,  $R_S$  of the diode [51]. To maximize the rectifier conversion efficiency, it is desired that the diode has a low junction capacitor, low series resistor, and high breakdown voltage. However, achieving all three simultaneously in one diode is quite impossible due to the involved physical mechanisms in the diodes and their intercorrelation

[51]. Additionally, the diode should have a low threshold voltage,  $V_{TH}$ , and offer a high reverse saturation current,  $I_S$  [52]. Table 11 summarizes important parameters of the most commonly used Schottky diodes in rectifiers for RF energy harvesting [53].

**Table 11.** Manufacturer characteristic parameters of most commonly used Schottky diodes in energy harvesting [53].

Diode	Vth (V)	Rs ( $\Omega$ )	Cjo (pF)	Is ( $\mu$ A)	BV (V)
MA4E1317	0.70	4	0.02	0.1	7.0
HSMS 2852	0.15	25	0.18	3.0	3.8
HSMS 2850	0.15	25	0.18	3.0	3.8
HSMS 2860	0.25	6.0	0.18	0.05	7.0
HSMS 286B	0.69	6	0.18	0.05	7.0
HSMS 2820	0.15	6	0.70	0.022	15.0
SMS 7630-079LF	0.09	20	0.14	5.0	2.0

SMS7630-079LF and HSMS-2850 exhibit the highest reverse saturation currents, with that of SMS-7630 being higher. Both diodes also feature low zero-bias junction capacitors, although HSMS-2850 has the lowest value. SMS-7630 offers the lowest threshold voltage, which is slightly lower than that of HSMS-2850. However, both diodes have low breakdown voltages, with that of HSMS-2850 slightly higher. On the other hand, HSMS-2820 has the highest breakdown voltage but is unsuitable due to its very low saturation current and high junction capacitance. HSMS-2850 and SMS7630-079LF diodes are chosen as ideal candidates for this work. However, for the sake of comparison and completion, HSMS2860 is also considered. Although HSMS-2860 has almost twice the threshold voltage of HSMS-2850 and SMS7630-079LF, it boasts twice the breakdown voltage and a low series resistor. Furthermore, HSMS-2850 and HSMS-2860 benefit from a more accurate vendor model for ADS simulation software. In the initial design, HSMS-2860 is used as the rectifying element, and the voltage doubler topology is selected to increase the output power. The study of the literature shows that a single-stage voltage doubler topology increases the output voltage by a factor of two.

An open-circuit stub is used in a T-matching network to match a  $50 \Omega$  input RF generator to the rectifier (Figure 19). The open-circuit stub behaves as an inductance of value  $L$  since the calculated reactive value is positive. The length of the open circuit is calculated using Equation (10). The length is further optimized through simulation. The input impedance of a lossless open-circuit stub is given by Equation (9).

$$Z_{cc} = jZ_0 \tan\left(\frac{2l\pi}{\lambda_g}\right) \quad (9)$$

$$l = \left(\frac{\lambda_g}{2\pi}\right)(n\pi + \arctan(\omega L/Z_0)) \quad (10)$$

where  $\lambda_g$  and  $Z_0$  represent the guided wavelength and characteristics impedance, respectively.

A closed DC loop for current circulation is shown in Figure 19. The rectifier is designed at 2.45 GHz with an input power of -10 dBm. The model of the via in [54] is adopted. To block unrectified RF signals from reaching the load, a choke inductance of 1 mH is used as a safe measure.

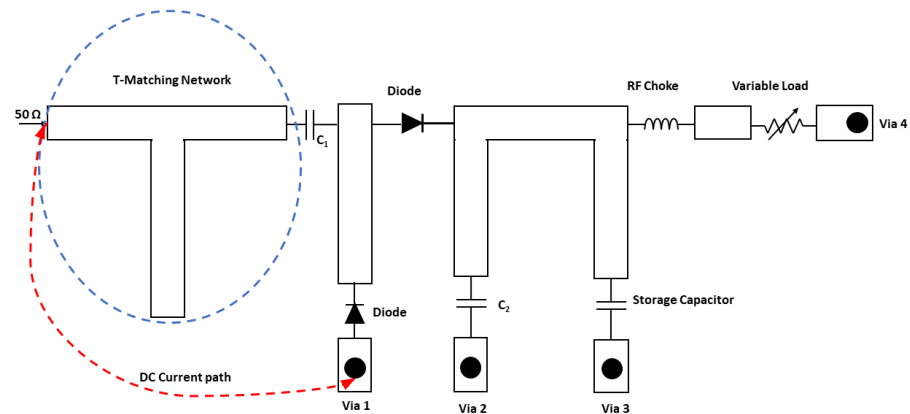


**Figure 19.** Rectifier schematics based on the voltage-doubler topology with complete DC path.

4.1. Simulation and Measurement Setup

The rectifier schematic was captured and validated using ADS momentum following the following steps.

1. The simulation layout is generated from the schematic design software. Pins' effects are added as lump components at the various gaps between the ground and input power supply.
2. The cardboard substrate model is adjusted with the RF properties obtained from characterization in Section 2 (Figure 20 (top)).
3. The frequency range is set between 2 GHz and 3 GHz in the momentum co-simulation.
4. The lumped components, ground, power supply, via-ground, and via-inductor are connected to the schematic in (Figure 20 (bottom)).

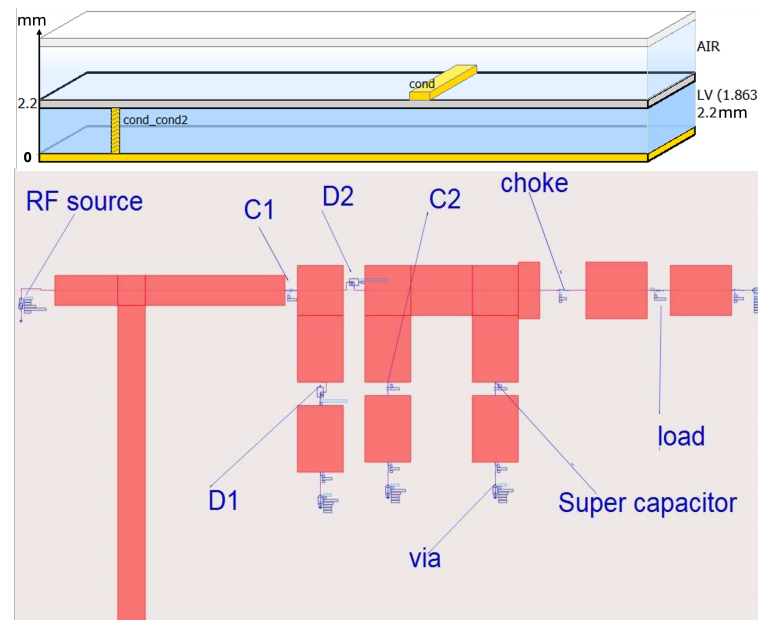


**Figure 20.** Schematics of the rectifier in Figure 19 for momentum co-simulation with configuration for cardboard sample #1 substrate.

A previous work [6] details how matching was performed and describes how co-simulation is performed. To ensure that the rectifier is supplied with the intended input power (−10 dBm, −5 dBm, 0 dBm), directional couplers are utilized in the measurement setup (Figure 21). The incident power,  $P_i$ , is evaluated using the RF generator, but some losses,  $P_l$ , exist from the connecting devices. To obtain reliable results, the losses from

the coupler, measuring cables, and connectors are measured before the experiment. The reflected power, the input power, and the losses are used to calculate the power transmitted to the rectifier ( $P_t$ ) with the help of Equation (11). The incident power from the RF generator ( $P_i$ ) is adjusted until the calculated transmitted power reaches the desired value for characterization. That is, if the rectifier is designed and optimized at -10 dBm, the incident power is adjusted until the calculated transmitted power reaches -10 dBm. This way, we ensure that the rectifier is supplied with -10 dBm. A voltmeter with high internal impedance is used to measure the rectified DC voltage across the DC load.

$$P_t = P_i - P_r - P_l \tag{11}$$

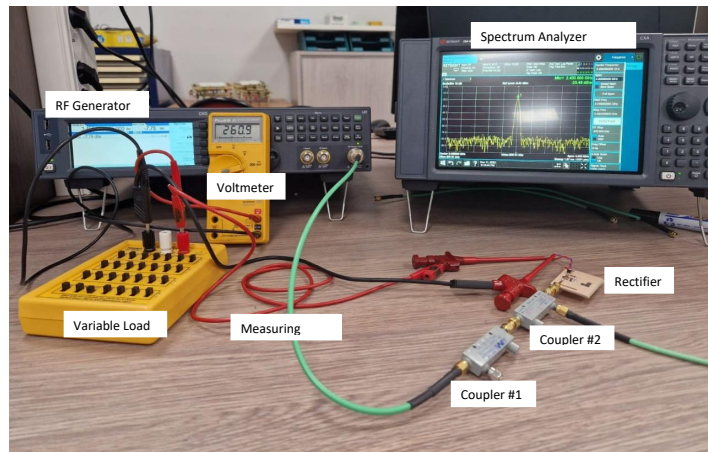
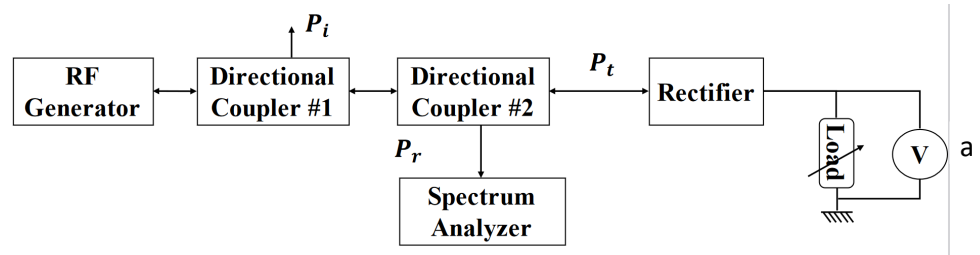


**Figure 21.** Laboratory setup for measuring the rectified voltage of cardboard rectifier at 2.45 GHz under varying load and input power conditions: (a) schematics, (b) lab setup.

4.2. Results

The fabricated rectifier is shown in Figure 22.

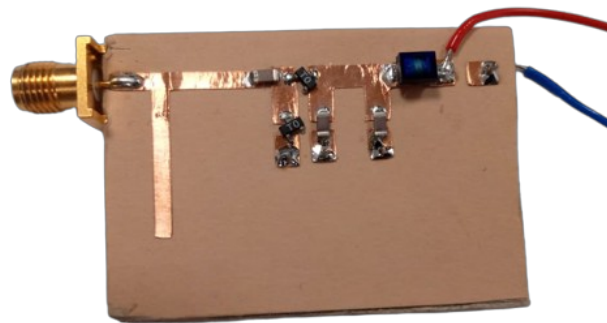


**Figure 22.** Fabricated rectifier on cardboard sample #1a using HSMS-2860 diode according to the schematic in Figure 20 (bottom).

The simulated and measured return loss of the rectifier, respectively, at -10 dBm and -5 dBm are depicted in Figure 23. Notably, there is a leftward shift in the measured results.

This shift may be partly attributed to the dielectric constant of the cardboard material, which is not constant. The diode impedance depends also on the current level. At 2.45 GHz a good match is obtained for the measurements at the three input power values. There is a shift to the left in the measured results. This shift may be partly attributed to the dielectric constant of the cardboard material which is not constant. The diode impedance also depends on the current level. At 2.45 GHz a good match is obtained for the measurements at the three input power values.

$$P_{DC} = \frac{V_{dc}^2}{R_L} \tag{12}$$

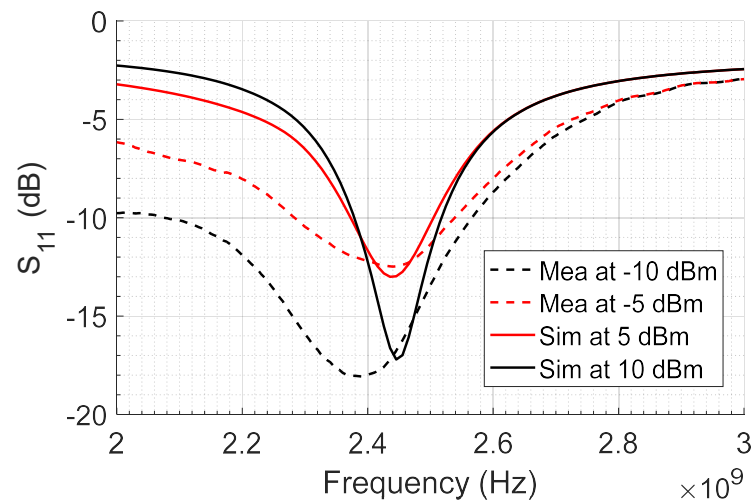


**Figure 23.** Simulated and measured  $S_{11}$  under different input power conditions of rectifier fabricated on cardboard sample #1.

To determine the maximum power point (MPP) conditions, the DC load is varied from 0.5 kΩ to 40 kΩ while adjusting the power source level to ensure a fixed power level at the rectifier input, and the DC voltage is measured. The DC power is calculated from the measured DC voltage (Figure 24).

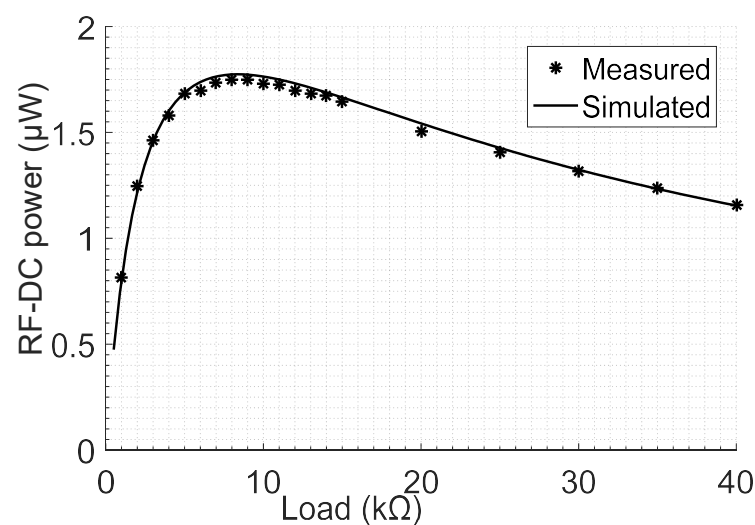


**Figure 24.** Simulated and measured DC output power of cardboard sample #1 rectifier in Figure 22 under −10 dBm input RF power at 2.45 GHz.

Figure 24 demonstrates that the measurement under  $-10$  dBm input RF power follows a similar tendency to the simulation, with little discrepancy between the two. Both results show that the MPP condition is attained when the load value is  $8$  k $\Omega$ . This corresponds to a measured output DC power of  $1.73$   $\mu$ W.

#### 4.3. Impact of Diodes on Rectifier Designed on Cardboard Substrate

Three identical rectifiers are designed and fabricated using SMS7630-079LF, HSMS-2850, and HSMS-2860 diode, respectively, on cardboard material #1. The MPP conditions are investigated for each rectifier, i.e., diode. The fabricated circuits with the three different diodes are shown in Figure 25.

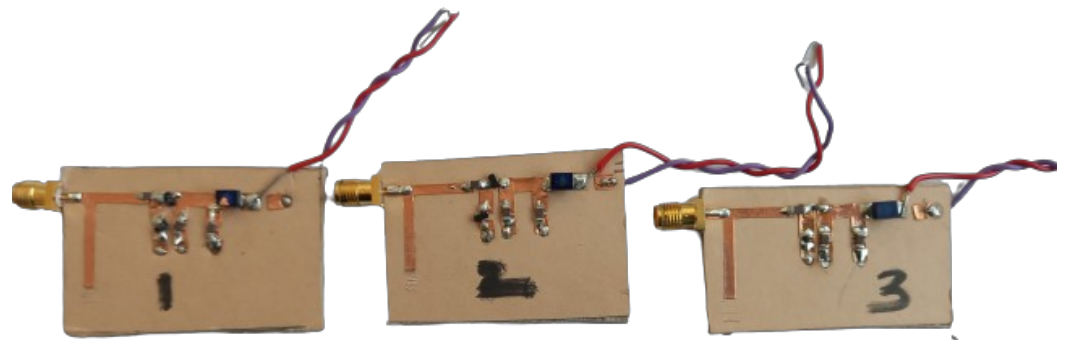


**Figure 25.** Rectifiers with three different diodes on cardboard material #1a: (1) HSMS-2860, (2) HSMS-2850, (3) SMS7630-079LF 7630.

Before proceeding with the analysis, we ensured that all circuits with different diodes were well matched at  $2.45$  GHz.

The plot in Figure 26 shows the measured output power versus load for all three rectifiers under  $-10$  dBm of RF input power.

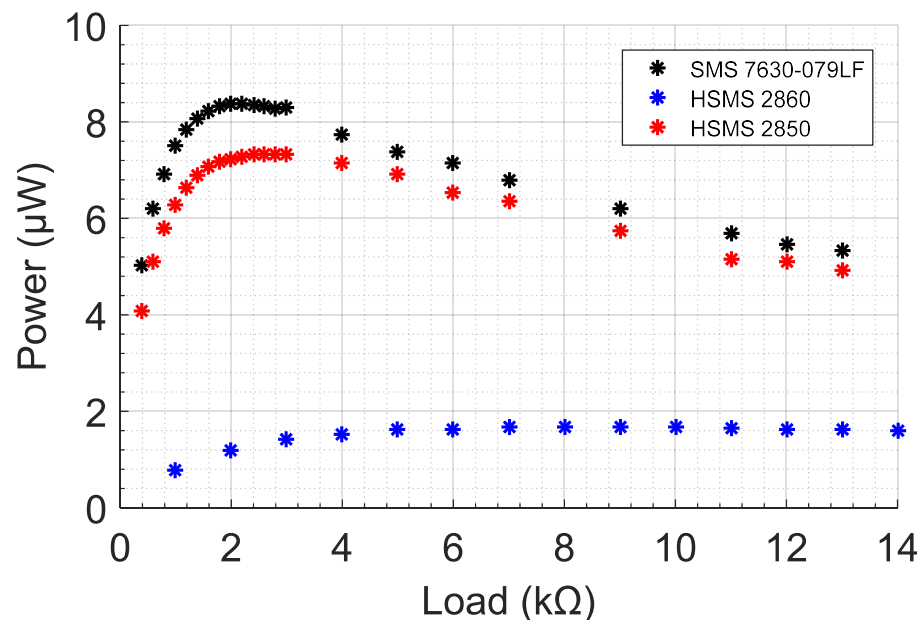


**Figure 26.** Output DC power versus load for rectifiers in Figure 25 under  $-10$  dBm input power.

Other measurements were performed at input power levels of  $0$  dBm and  $-5$  dBm, respectively (Figures 27 and 28).

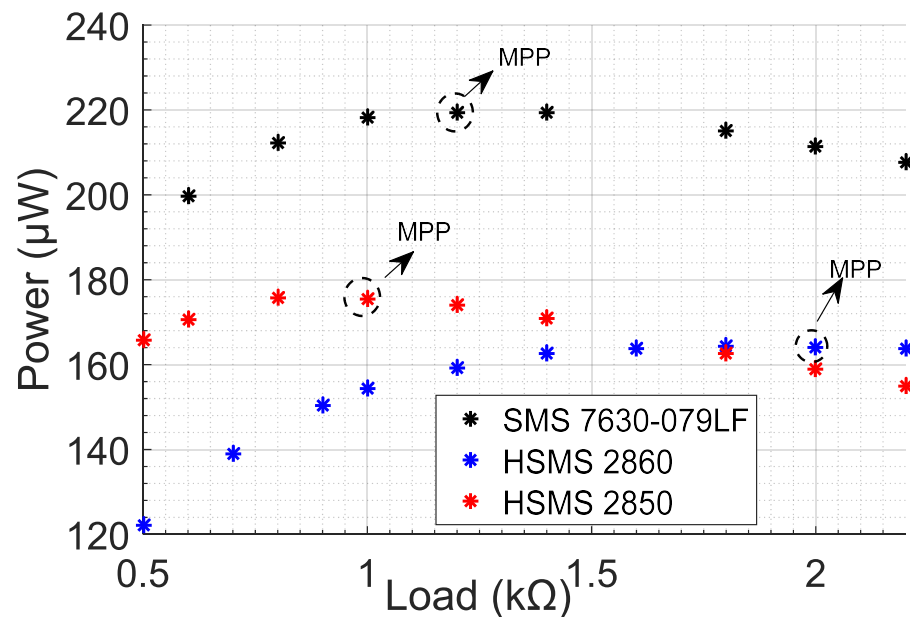


Figure 27. Measured RF–DC output power under 0 dBm input power for rectifiers in Figure 25.

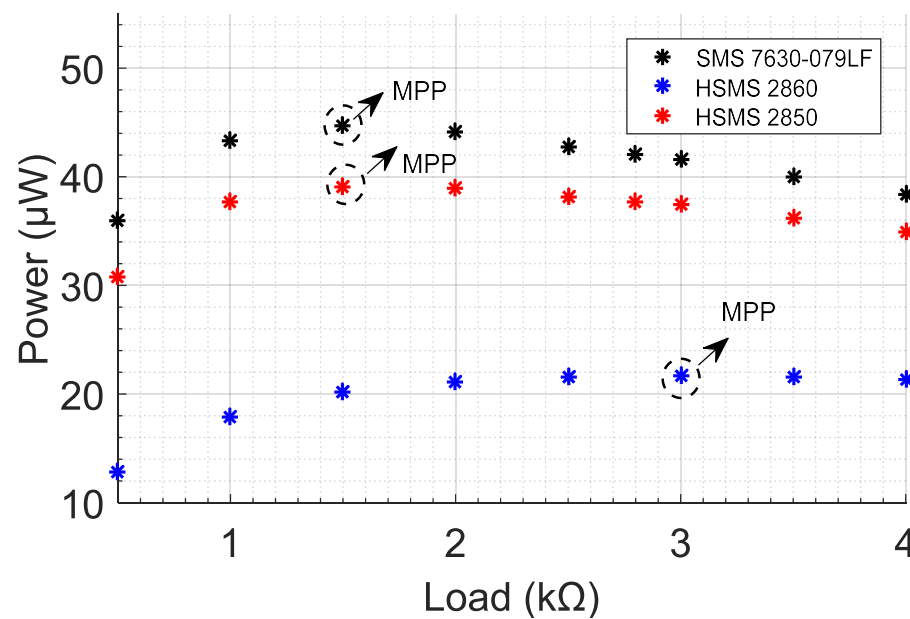


Figure 28. Measured RF–DC output power under  $-5$  dBm of input power for rectifiers in Figure 25.

Irrespective of the input power, the rectifier with the SMS7630-079LF diode offers the highest output DC power, closely followed by the HSMS-2850 diode. As the RF input power increases, the optimal load decreases for all three diodes (Table 12). This is because the increase in RF input power leads to an increase in DC current, leading to better diode direct polarization, hence reducing some losses.

**Table 12.** Optimal output load values in  $k\Omega$  for rectifiers with HSMS-2850, HSMS-2860, and SMS7630-079LF diodes under different input power levels.

Power (dBm)	SMS7630-079LF	HSMS-2850	HSMS-2860
0	1.1	1	2
-5	1.5	1.5	3
-10	2	2.6	8

4.4. Impact of the Substrate on Rectifier Operation

The impact of the substrate on rectifier operation is also investigated. Three rectifiers were fabricated on Rogers RO4003C, PLA, and cardboard substrate #1, respectively, and using SMS7630-079LF. The fabricated circuits are shown in Figure 29. The measurement setup is performed without the directional coupler in Figure 21 since we are interested in the losses of each substrate. The measured results of output DC power versus load under 0 dBm, -5 dBm, and -10 dBm, respectively, are shown in Figures 30–32.

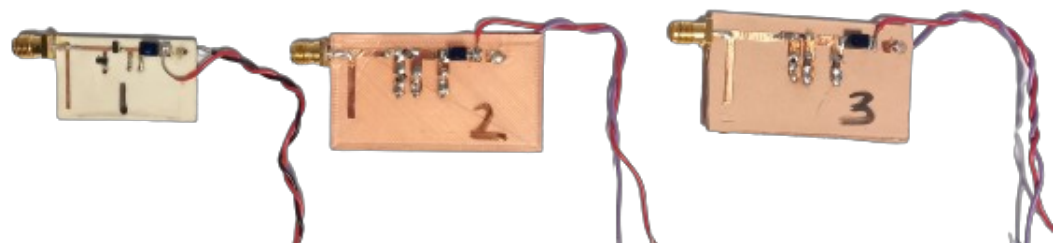


**Figure 29.** Rectifiers on three different substrates but the same SMS7630-079LF diodes: (1) Rogers RO4003C, (2) PLA (3) cardboard #1.

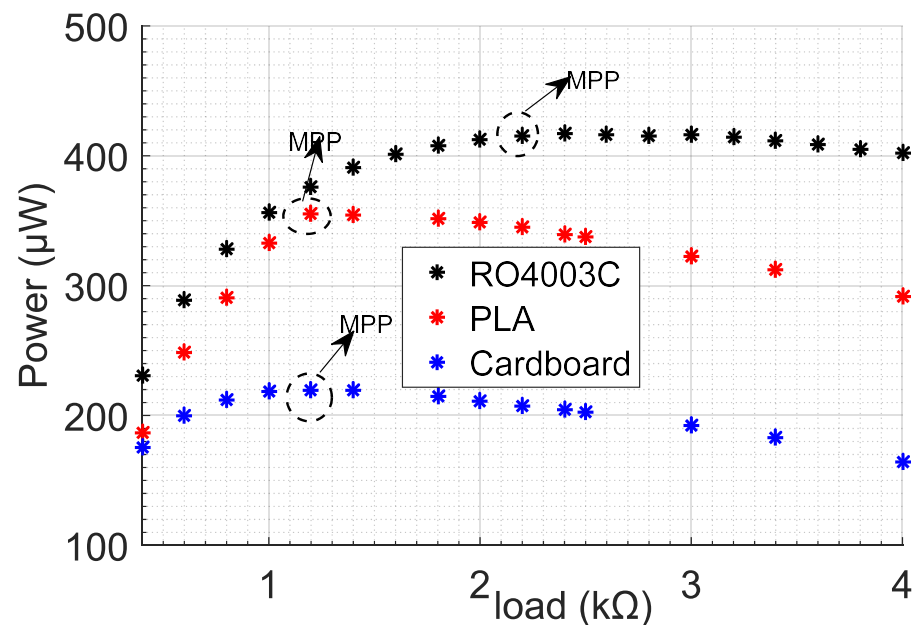


**Figure 30.** Measured RF–DC power under varying load and 0 dBm of input RF power for rectifiers in Figure 29.



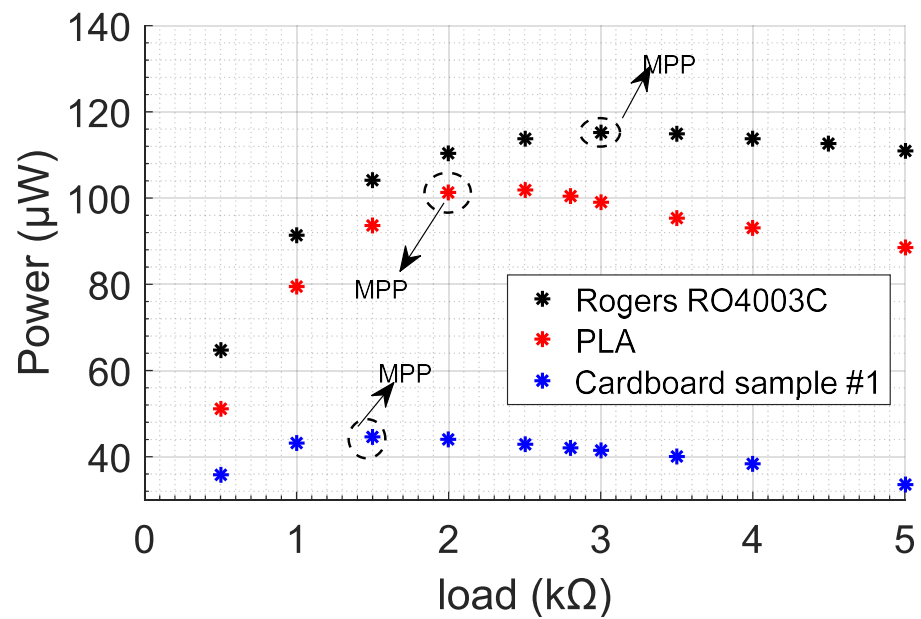


Figure 31. Measured RF–DC power under varying load and -5 dBm of input RF power for rectifiers in Figure 29.

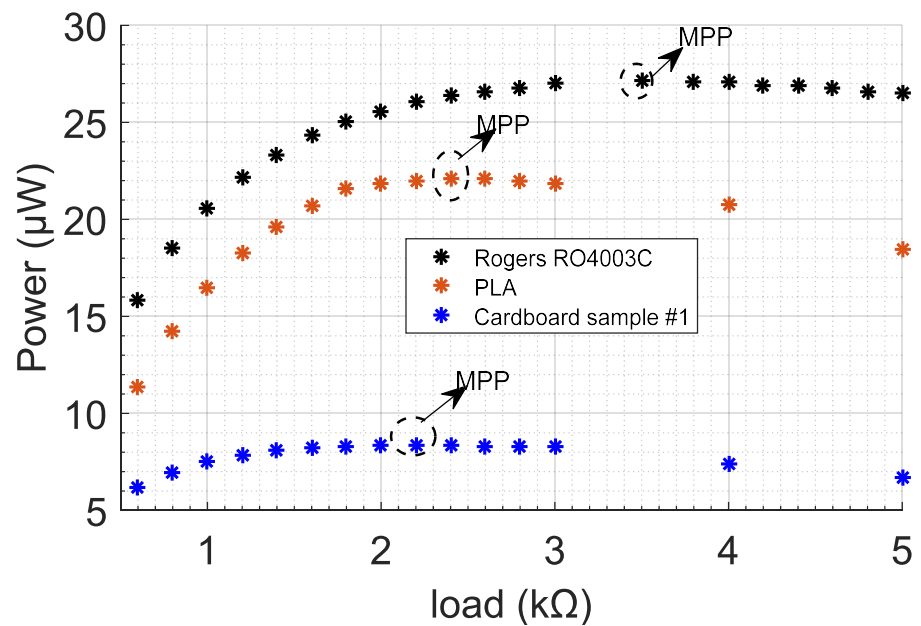


Figure 32. Measured RF–DC power under varying load and -10 dBm of input RF power for rectifiers in Figure 29.

As expected and summarized in Table 13, the rectifier designed on Rogers substrate gives the best results, followed by the one on PLA substrate and cardboard material. This is due to the lowest loss tangent of Rogers substrate (0.0027), which is around four times lower than the one of PLA (0.01) [6], which is also approximately six times lower than the loss tangent of cardboard material #1 (0.055). Despite the lowest value of DC power, the rectifier on cardboard material offers acceptable operation within the range of power obtained for RF energy harvesting solutions (Table 13). This shows that even with cheap, recyclable, and eco-friendly substrates, RF energy harvesting circuits can still be manufactured. PLA and cardboard materials are cheap, eco-friendly, and recyclable, thus permitting the implementation of wireless service at low cost.

Table 13. Comparison of rectifier output performances.

Freq. (GHz)	Pin (dBm)@Load (kΩ)	PCE@RF–DC Power (μW)	Substrate/Print Tech	Size (mm <sup>3</sup> )	Ref
2.45	0 @ 5	39.2%@392	Rogers RT/Duroid 5880/PCB	60 × 40 × 1.57	[21]
2.45	0 @ 7	50%@500	LCP/not mentioned	15.1 × 8.15 × 0.18	[25]
2.3	−24 @ 14.7	5%@0.2	FR4/printed circuit board	70 × 70 × 13.2	[8]
2.45	−20 @ 20	6%@0.6	Rogers RT (Duroid) 5880/printed circuit board	60 × 40 × 1.57	[21]
2.45	−15@1.7 −20 @ 2 −25 @ 3.9	19%@ 6 24%@0.96 5%@0.14	PLA/fuse deposition modeling 3D printing polymer	42 × 14 × 1.5	[6]
2.45	0 @ 2.4 −5@3 −10 @ 3.5	41.5%@ 415 36.4%@115 27.5%@27.5	Rogers RO4003C/PCB	35 × 17 × 1.5	This work
2.45	0 @1.1 −5 @ 1.5 −10@2	22%@ 220 14.2%@45 8.5%@8.5	Cardboard #1/copper tape	50 × 20 × 2.2	This work

## 5. Conclusions

The use of waste cardboard paper material for constructing a rectenna was investigated based on a simple fabrication scheme, ready to easily dismantle the fabricated objects. The electrical traces in all designs were realized with a commercial copper tape of thickness 35 μm. The copper tape is meant to be removed easily from the surface of objects. The cardboard substrates and the fabrication process introduced constraints in the design of a rectenna. This paper aimed to document design parameters and performance metrics.

The first step was to extract the loss tangent and relative permittivity of the material. There are many types of cardboard materials, depending on their thickness, surface roughness, and air gaps. This paper provided the details of the characterization method for four different material substrates. The identified RF properties were used in the design of the antenna and the rectifier, respectively. A microstrip patch antenna was designed to resonate in the 2.45 GHz ISM band. This paper confirmed that an increase in the captured EM waves leads to higher PCE by designing a dual-band microstrip patch antenna at 900 MHz and 1800 MHz bands. The limitation in the bandwidth of the microstrip patch antenna was corrected by designing a monopole antenna of broadband width.

The paper did not introduce any original design contribution; rather, it demonstrated that well-known design approaches do operate successfully with the selected cardboard substrates and are not impacted by the simple fabrication process. The rectifier is a single-stage voltage multiplier because it can double the rectified voltage theoretically when the incoming RF power is sufficient (PCE of 14.2% at −5 dBm input power). Under −10 dBm input RF power, nearly 1.7 μW DC output power is available for the smallest experimented patch antenna.

The power supply of microwatt wireless sensors is covered by the literature [55]. It appears that both the antenna and the rectifier offer some level of performance below the ones of counterparts fabricated on Rogers' substrate. This is not surprising, and the lower performances are experimentally verified and easily explained. However, the available DC output power under a decent level of RF input power enables us to consider the supply

tiny systems to some extent, benefiting from the ecological aspects of recycled cardboard. Moreover, folding the substrate to accommodate particular geometry constraints of the object may be considered.

**Author Contributions:** Methodology, J.V.; validation, J.-M.D.; formal analysis, A.P.; investigation, P.U.L.; resources, T.G., P.L.; writing—original draft preparation, B.A.; writing—review and editing, P.B., F.M., M.C.; supervision, B.A.; project administration, P.T. All authors have read and agreed to the published version of the manuscript.

**Funding:** This research received no external funding.

**Data Availability Statement:** No data available.

**Acknowledgments:** The authors wish to thank the support of Region Auvergne-Rhone-Alpes, GIP CNFM and ANR AMI CMA INFORISM regarding 3D Plastronics platform.

**Conflicts of Interest:** The authors declare no conflicts of interest.

## References

1. Sleebi, K.; Divakaran, D.D.K.; Nasimuddin. RF energy harvesting systems: An overview and design issues. *Int. J. Microw. Comput. Eng.* **2019**, *29*, e21633.
2. A Comprehensive Review of Metasurface Structures Suitable for RF Energy Harvesting. *IEEE Access* **2020**, *8*, 76433–76452.
3. Georgiadis, A.; Collado, A.; Via, S.; Meneses, C. Flexible hybrid solar/EM energy harvester for autonomous sensors. In Proceedings of the IEEE MTT-S International Microwave Symposium Digest, Baltimore, MD, USA, 5–10 June 2011; pp. 6–9. <https://doi.org/10.1109/MWSYM.2011.5972963>.
4. Palazzi, V.; Kalialakis, C.; Alimenti, F.; Mezzanotte, P.; Roselli, L.; Collado, A.; Georgiadis, A. Performance analysis of a ultra-compact low-power rectenna in paper substrate for RF energy harvesting. In Proceedings of the 2017 IEEE Topical Conference on Wireless Sensors and Sensor Networks (WiSNet), Austin, TX, USA, 24–27 January 2017; IEEE: Piscataway, NJ, USA, 2017; pp. 65–68.
5. Issa, H.; Wehbi, M.; Kaddour, D. Low-cost environment-friendly energy scavenging system. *Eng. Res. Express* **2023**, *5*, 025040.
6. Linge, P.U.; Gerges, T.; Bevilacqua, P.; Duchamp, J.M.; Benech, P.; Verdier, J.; Lombard, P.; Cabrera, M.; Tsafack, P.; Mieyeville, F.; et al. Evaluation of Polylactic Acid Polymer as a Substrate in Rectenna for Ambient Radiofrequency Energy Harvesting. *J. Low Power Electron. Appl.* **2023**, *13*, 34.
7. Muhammad, S.; Tiang, J.J.; Wong, S.K.; Smida, A.; Ghayoula, R.; Iqbal, A. A Dual-Band Ambient Energy Harvesting Rectenna Design for Wireless Power Communications. *IEEE Access* **2021**, *9*, 99944–99953. <https://doi.org/10.1109/ACCESS.2021.3096834>.
8. Song, C.; Huang, Y.; Zhou, J.; Zhang, J.; Yuan, S.; Carter, P. A high-efficiency broadband rectenna for ambient wireless energy harvesting. *IEEE Trans. Antennas Propag.* **2015**, *63*, 3486–3495. <https://doi.org/10.1109/TAP.2015.2431719>.
9. Linh Nguyen, X.V.; Gerges, T.; Duchamp, J.M.; Benech, P.; Verdier, J.; Lombard, P.; Cabrera, M.; Allard, B. Stereolithography-Based Rectenna for Wireless Energy Harvesting. In Proceedings of the 2021 IEEE 34th International System-on-Chip Conference (SOCC), Las Vegas, NV, USA, 14–16 September 2021; pp. 34–39, ISSN: 2164-1706. <https://doi.org/10.1109/SOCC52499.2021.9739329>.
10. Palazzi, V.; Hester, J.; Bito, J.; Alimenti, F.; Kalialakis, C.; Collado, A.; Mezzanotte, P.; Georgiadis, A.; Roselli, L.; Tentzeris, M.M. A Novel Ultra-Lightweight Multiband Rectenna on Paper for RF Energy Harvesting in the Next Generation LTE Bands. *IEEE Trans. Microw. Theory Tech.* **2018**, *66*, 366–379. <https://doi.org/10.1109/TMTT.2017.2721399>.
11. Awais, Q.; Jin, Y.; Chattha, H.T.; Jamil, M.; Qiang, H.; Khawaja, B.A. A Compact Rectenna System With High Conversion Efficiency for Wireless Energy Harvesting. *IEEE Access* **2018**, *6*, 35857–35866. <https://doi.org/10.1109/ACCESS.2018.2848907>.
12. Roy, S.; Tiang, J.J.; Roslee, M.B.; Ahmed, M.T.; Kouzani, A.Z.; Mahmud, M.P. Quad-band rectenna for ambient radio frequency (RF) energy harvesting. *Sensors* **2021**, *21*, 7838.
13. Hucheng Sun.; Yong-xin Guo.; Miao He.; Zheng Zhong. A dual-band rectenna using broadband yagi antenna array for ambient rf power harvesting. *IEEE Antennas Wirel. Propag. Lett.* **2013**, *12*, 918–921. <https://doi.org/10.1109/LAWP.2013.2272873>.
14. Roy, S.; Tiang, J.J.; Roslee, M.B.; Ahmed, M.T.; Kouzani, A.Z.; Mahmud, M.P. Design of a Highly Efficient Wideband Multi-Frequency Ambient RF Energy Harvester. *Sensors* **2022**, *22*, 424.
15. Hamidouche, A.M.; Takhedmit, H.; Poulichet, P.; Cirio, L. Efficiency improvement of an UWB rectifier by using optimized pulse modulation signal: Simulation and experiments. In Proceedings of the 2022 Wireless Power Week (WPW), Bordeaux, France, 5–8 July 2022; pp. 407–411. <https://doi.org/10.1109/WPW54272.2022.9853893>.
16. Nguyen, X.V.L.; Gerges, T.; Duchamp, J.M.; Benech, P.; Verdier, J.; Lombard, P.; Cabrera, M.; Allard, B. 3D Plastronics Radio Frequency Energy Harvester on Stereolithography Parts. In Proceedings of the 2022 Wireless Power Week (WPW), Bordeaux, France, 5–8 July 2022; pp. 156–161. <https://doi.org/10.1109/WPW54272.2022.9854010>.
17. Niotaki, K.; Kim, S.; Jeong, S.; Collado, A.; Georgiadis, A.; Tentzeris, M.M. A Compact Dual-Band Rectenna Using Slot-Loaded Dual Band Folded Dipole Antenna. *IEEE Antennas Wirel. Propag. Lett.* **2013**, *12*, 1634–1637.
18. Shen, S.; Chiu, C.Y.; Murch, R.D. A dual-port triple-band L-probe microstrip patch rectenna for ambient RF energy harvesting. *IEEE Antennas Wirel. Propag. Lett.* **2017**, *16*, 3071–3074. <https://doi.org/10.1109/LAWP.2017.2761397>.

19. Lin, C.H.; Chiu, C.W.; Gong, J.Y. A Wearable Rectenna to Harvest Low-Power RF Energy for Wireless Healthcare Applications. In Proceedings of the 2018 11th International Congress on Image and Signal Processing, BioMedical Engineering and Informatics (CISP-BMEI), Beijing, China, 13–15 October 2018; pp. 1–5. <https://doi.org/10.1109/CISP-BMEI.2018.8633222>.
20. Mansour, M.M.; Kanaya, H. Compact RF rectifier circuit for ambient energy harvesting. In Proceedings of the 2017 IEEE International Symposium on Radio-Frequency Integration Technology, RFIT 2017, Seoul, Republic of Korea, 30 August–1 September 2017; pp. 220–222. <https://doi.org/10.1109/RFIT.2017.8048256>.
21. Ur Rehman, M.; Ahmad, W.; Khan, W.T. Highly efficient dual band 2.45/5.85 GHz rectifier for RF energy harvesting applications in ISM band. In Proceedings of the Asia-Pacific Microwave Conference Proceedings, APMC, Kuala Lumpur, Malaysia, 13–16 November 2017; pp. 150–153. <https://doi.org/10.1109/APMC.2017.8251400>.
22. Tafekirt, H.; Pelegri-Sebastia, J.; Bouajaj, A.; Reda, B.M. A Sensitive Triple-Band Rectifier for Energy Harvesting Applications. *IEEE Access* **2020**, *8*, 73659–73664. <https://doi.org/10.1109/ACCESS.2020.2986797>.
23. Almoneef, T.S. Design of a Rectenna Array without a Matching Network. *IEEE Access* **2020**, *8*, 109071–109079. <https://doi.org/10.1109/ACCESS.2020.3001903>.
24. Eid, A.; Costantine, J.; Tawk, Y.; Ramadan, A.H.; Abdallah, M.; Elhajj, R.; Awad, R.; Kasbah, I.B. An efficient RF energy harvesting system. In Proceedings of the 2017 11th European Conference on Antennas and Propagation, EUCAP 2017, Paris, France, 19–24 March 2017; pp. 896–899. <https://doi.org/10.23919/EuCAP.2017.7928573>.
25. Eid, A.; Hester, J.G.; Costantine, J.; Tawk, Y.; Ramadan, A.H.; Tentzeris, M.M. A Compact Source-Load Agnostic Flexible Rectenna Topology for IoT Devices. *IEEE Trans. Antennas Propag.* **2020**, *68*, 2621–2629. <https://doi.org/10.1109/TAP.2019.2955211>.
26. Papadopoulou, M.S.; Boursianis, A.D.; Volos, C.K.; Stouboulos, I.N.; Nikolaidis, S.; Goudos, S.K. High-Efficiency Triple-Band RF-to-DC Rectifier Primary Design for RF Energy-Harvesting Systems. *Telecom* **2021**, *2*, 271–284. <https://doi.org/10.3390/telecom2030018>.
27. Khonsari, Z.; Björninen, T.; Tentzeris, M.M.; Sydänheimo, L.; Ukkonen, L. 2.4 GHz inkjet-printed RF energy harvester on bulk cardboard substrate. In Proceedings of the 2015 IEEE Radio and Wireless Symposium (RWS), San Diego, CA, USA, 25–28 January 2015; pp. 153–155, ISSN: 2164-2974, <https://doi.org/10.1109/RWS.2015.7129721>.
28. Mouapi, A.; Hakem, N.; Kandil, N.; Kamani, G.V. A Miniature Rectifier Design for Radio Frequency Energy Harvesting Applied at 2.45 GHz. In Proceedings of the 2018 IEEE International Conference on Environment and Electrical Engineering and 2018 IEEE Industrial and Commercial Power Systems Europe, EEEIC/I and CPS Europe 2018, Palermo, Italy, 12–15 June 2018; pp. 1–5. <https://doi.org/10.1109/EEEIC.2018.8493844>.
29. Asakura, S.; Yamanokuchi, S.; Yoshida, S.; Nishikawa, K. Design and Prototyping of a Single-Shunt Rectifier with 71% Fractional Bandwidth Having Acceptable Matching on 10 dBm LSSP. In Proceedings of the 2022 Wireless Power Week (WPW), Bordeaux, France, 5–8 July 2022; pp. 383–387. <https://doi.org/10.1109/WPW54272.2022.9853949>.
30. Hoque, M.U.; Kumar, D.; Audet, Y.; Savaria, Y. Design and Analysis of a 35 GHz Rectenna System for Wireless Power Transfer to an Unmanned Air Vehicle. *Energies* **2022**, *15*, 320. <https://doi.org/10.3390/en15010320>.
31. Kawai, K.; Takabayashi, N.; Toyonaga, T.; Suzuki, K.; Shinohara, N. Development of Rectenna for Estimating Received Power Level Using Second Harmonic Wave. In Proceedings of the 2022 Wireless Power Week (WPW), Bordeaux, France, 5–8 July 2022; pp. 175–179. <https://doi.org/10.1109/WPW54272.2022.9854024>.
32. Mangan, A.; Voinigescu, S.; Yang, M.T.; Tazlauanu, M. De-embedding transmission line measurements for accurate modeling of IC designs. *IEEE Trans. Electron Devices* **2006**, *53*, 235–241. <https://doi.org/10.1109/TED.2005.861726>.
33. Chang, S.H.; Kuan, H.; Wu, H.W.; Yang, R.Y.; Weng, M.H. Determination of microwave dielectric constant by two microstrip line method combined with EM simulation. *Microw. Opt. Technol. Lett.* **2006**, *48*, 2199–2201.
34. Das, N.K.; Voda, S.M.; Pozar, D.M. Two methods for the measurement of substrate dielectric constant. *IEEE Trans. Microw. Theory Tech.* **1987**, *35*, 636–642.
35. Saghlatoon, H.; Sydänheimo, L.; Ukkonen, L.; Tentzeris, M. Optimization of inkjet printing of patch antennas on low-cost fibrous substrates. *IEEE Antennas Wirel. Propag. Lett.* **2014**, *13*, 915–918.
36. Devi, K.K.A.; Din, N.M.; Chakrabarty, C.K. Optimization of the Voltage Doubler Stages in an RF-DC Converter Module for Energy Harvesting. *Circuits Syst.* **2012**, *3*, 216–222. <https://doi.org/10.4236/cs.2012.33030>.
37. Majumder, A. Rectangular Microstrip Patch Antenna Using Coaxial Probe Feeding Technique to Operate in S-Band. *Int. J. Eng. Trends Technol.* **2013**, *4*, 1206–1210.
38. Bernhard, J.; Mayes, P.; Schaubert, D.; Mailloux, R. A commemoration of Deschamps’ and Sichak’s ‘Microstrip microwave antennas’: 50 years of development, divergence, and new directions. In Proceedings of the 2003 Antenna Applications Symp, 2003; pp. 189–230.
39. Gutton, H.; Baissinot, G. Flat Aerial for Ultra High Frequencies. French Patent CA627967A, 26 September 1961.
40. Munson, R. Conformal microstrip antennas and microstrip phased arrays. *IEEE Trans. Antennas Propag.* **1974**, *22*, 74–78.
41. Howell, J. Microstrip antennas. *IEEE Trans. Antennas Propag.* **1975**, *23*, 90–93.
42. Derneryd, A. Linearly polarized microstrip antennas. *IEEE Trans. Antennas Propag.* **1976**, *24*, 846–851.
43. Shen, L.; Long, S.; Allarding, M.; Walton, M. Resonant frequency of a circular disc, printed-circuit antenna. *IEEE Trans. Antennas Propag.* **1977**, *25*, 595–596.
44. Agrawal, P.; Bailey, M. An analysis technique for microstrip antennas. *IEEE Trans. Antennas Propag.* **1977**, *25*, 756–759.

45. Derneryd, A. A theoretical investigation of the rectangular microstrip antenna element. *IEEE Trans. Antennas Propag.* **1978**, *26*, 532–535.
46. Derneryd, A. Analysis of the microstrip disk antenna element. *IEEE Trans. Antennas Propag.* **1979**, *27*, 660–664.
47. Din, N.M.; Chakrabarty, C.K.; Bin Ismail, A.; Devi, K.K.; Chen, W.Y. Design of RF energy harvesting system for energizing low power devices. *Prog. Electromagn. Res.* **2012**, *132*, 49–69. <https://doi.org/10.2528/pier12072002>.
48. Khan, A.; Nema, R. Analysis of five different dielectric substrates on microstrip patch antenna. *Int. J. Comput. Appl.* **2012**, *55*.
49. Rop, K.; Konditi, D. Performance analysis of a rectangular microstrip patch antenna on different dielectric substrates. *Innov. Syst. Des. Eng.* **2012**, *3*, 1727–1729.
50. Balanis, C.A. *Antenna Theory; Analysis and Design*, 4th ed.; IEEE: New York, NY, USA, 2016. <https://doi.org/10.1109/proc.1984.12959>.
51. Orlob, C.; Kornek, D.; Preihs, S.; Rolfes, I. Characterization of electromagnetic properties of molded interconnect device materials. In Proceedings of the 2009 German Microwave Conference, Munich, Germany, 16–18 March 2009; IEEE: Piscataway, NJ, USA, 2009; pp. 1–4.
52. Finkenzeller, K. *RFID Handbook: Fundamentals and Applications in Contactless Smart Cards, Radio Frequency Identification and Near-Field Communication*; John Wiley & Sons: Hoboken, NJ, USA, 2010.
53. Singh, D.; Sharma, M.; Yadav, S. Performance Comparison of Schottky Diode models for RF Energy Harvesting. *Int. J. Eng. Res. Appl.* **2020**, *10*, 51–57.
54. Marc E, Goldfarb, R.A.P. Modeling Via Hole Grounds in Microstrip. *IEEE Microw. Guid. Wave Lett.* **1991**, *1*, 135–137. <https://doi.org/10.1109/75.91090>.
55. Nimo, A.; Beckedahl, T.; Ostertag, T.; Reindl, L. Analysis of Passive RF-DC Power Rectification and Harvesting Wireless RF Energy for Micro-watt Sensors. *AIMS Energy* **2015**, *3*, 184–200. <https://doi.org/10.3934/energy.2015.2.184>.

**Disclaimer/Publisher’s Note:** The statements, opinions and data contained in all publications are solely those of the individual author(s) and contributor(s) and not of MDPI and/or the editor(s). MDPI and/or the editor(s) disclaim responsibility for any injury to people or property resulting from any ideas, methods, instructions or products referred to in the content.